

aPKC is A Key Polarity Molecule Coordinating the Function of Three Distinct Cell Polarities during Collective Migration

Heng Wang¹, Zhiqian Qiu¹, Zehao Xu¹, Samuel John Chen¹, Jun Luo¹, Xiaobo Wang^{2*}, Jiong Chen^{1*}

¹ State Key Laboratory of Pharmaceutical Biotechnology and MOE Key Laboratory of Model Animals for Disease Study, Model Animal Research Center, Nanjing University, 12 Xue-fu Road, Nanjing, China 210061

² LBCMCP, Centre de Biologie Intégrative (CBI), Université de Toulouse, CNRS, UPS, 31062 Toulouse, France

* Correspondence: chenjiong@nju.edu.cn; xiaobo.wang@univ-tlse3.fr

Tel: +86-25-58641507

Fax: +86-25-58641500

Keywords: Cell polarity, apical-basal polarity, collective cell migration, aPKC, Crumbs complex, *Drosophila* border cells.

Summary Statement

aPKC, spatially controlled by Crb complex, coordinates the generation of three distinct but inter-connected cell polarities during collective migration.

Abstract

Apical-basal polarity is a hallmark of epithelia and it needs to be remodeled when epithelial cells undergo morphogenetic cell movements. Here, we use border cells in *Drosophila* ovary to address how the apical-basal polarity is remodeled and turned into front-back, apical-basal and inside-outside polarities, during collective migration. We find that Crumbs (Crb) complex is required for the generation of the three distinct but inter-connected cell polarities of border cells. Specifically, Crb complex, together with Par complex and the endocytic recycling machinery, ensures a strict distribution control of two distinct populations of aPKC at the inside apical junction and near the outside lateral membrane respectively. Interestingly, aPKC distributed near the outside lateral membrane interacts with Tiam1/Sif and promotes the Rac-induced protrusions, whereas alteration of the aPKC distribution pattern changed protrusion formation pattern, leading to disruption of all three polarities. Therefore, we demonstrate that aPKC, spatially controlled by Crb complex, is a key polarity molecule coordinating the generation of three distinct but inter-connected cell polarities during collective migration.

Introduction

During animal development, cells display various forms of polarity or asymmetry, and how these cells establish, maintain, and remodel their cell polarity is a fundamental question in cell biology. One of the most common forms of cell polarity observed in developing organisms is the apical-basal polarity found in epithelial tissues (Tepass, 2012). Early discoveries of key polarity complexes are critical to the molecular understanding of the apical-basal polarity. They include the apically localized Par complex (aPKC/Par6/Par3/Cdc42) and Crb complex (Crb/Sdt/Patj), and the lateral complex of Scribble/Dlg/Lgl in *Drosophila*. However, recent works have found that individual components within the same complex, such as Crb or Par complex, may function differently in varying developmental stages or contexts (Knust and Bossinger, 2002; Morais-de-Sa et al., 2010; Penalva and Mirouse, 2012; Pocha and Knust, 2013; St Johnston and Ahringer, 2010; Tepass, 2012). As the epithelia undergo epithelial morphogenesis or collective cell movement, the original apical-basal polarity has to be remodeled and other types of cell polarity such as front-back polarity have to form (Tepass, 2012; Veeman and McDonald, 2016). However, the molecular mechanisms underlying such polarity remodeling is not well understood.

The border cells (BCs) in *Drosophila* ovary represent an excellent developmental system to study cell polarity generation and remodeling. They are genetically tractable and amenable to live cell imaging and optogenetic manipulation (Montell et al., 2012). And they have been used as an established *in vivo* model in the field of collective cell migration (Friedl and Gilmour, 2009). The BCs are derived from a group of about 6 follicle cells, which are part of the follicle epithelial layer that maintains its own apical-basal polarity (Fig. 1A) (Montell, 2003; Montell et al., 2012). As these follicle cells detach from their neighbors, round up, and form a migratory cluster, a dramatic polarity remodeling process takes place, resulting in three distinct cell polarities (Montell et al., 2012; Veeman and McDonald, 2016). First, the border cell cluster adopts a front-back polarity in distribution of actin cytoskeleton, signaling molecules and trafficking vesicles (Montell et al., 2012; Wan et al., 2013). The leading border

cell extends a major lamellipodial protrusion enriched in F-actin and actin dynamics regulators including active Rac and cofilin, whereas border cells at the side and back of the cluster only occasionally extend minor protrusions that contain less of them (Wang et al., 2010; Zhang et al., 2011). Such front-back polarity of actin cytoskeleton is established and maintained as a result of guidance signaling from two RTKs (Receptor Tyrosine Kinase), namely PVR (PDGFR and VEGFR related) and EGFR, with PVR making the major contribution (Montell, 2003; Montell et al., 2012). In addition, PVR is also mainly responsible for the asymmetric distribution of recycling endosome, exocyst and p-Tyr staining (Wan et al., 2013), which serves as a well-tested marker for intracellular signaling molecules.

The second polarity inherent in each of the 6 outer border cells and the 2 central polar cells is the apical-basal polarity (Fig. 1A), which has its origin in the follicle epithelial cells but is significantly remodeled to reflect the part-epithelial and part-mesenchymal characteristics of cells undergoing collective migration (Felix et al., 2015; Friedl and Gilmour, 2009; Niewiadomska et al., 1999; Pinheiro and Montell, 2004). Interestingly, outer border cells only extend their protrusions in their lateral membrane regions (Fig. 2) (Montell et al., 2012; Veeman and McDonald, 2016). But the functional significance of such restriction of protrusion formation only in the lateral region and not in the apical or basal region is not clear.

The third cell polarity within each outer border cell is the inside-outside polarity (Fig. 3D, Fig. 4H), which is much less understood in the field of cell polarity. The inside region is the membrane area where individual border cell attaches to polar cells and other neighboring border cells, while the outside region is the membrane region where border cells contact the surrounding substrate, the large nurse cells (Montell et al., 2012; Veeman and McDonald, 2016). It was known that F-actin, myosin II and E-cadherin clearly display polarized distribution at the outside or inside membrane (Cai et al., 2014; Combedazou et al., 2017; Lucas et al., 2013), which allows strong actin dynamics and protrusion formation to occur only at outside membrane of border

cells. But how does the original apical-basal polarity of follicle cells give rise to the three distinct cell polarities in the border cells? Is there a common mechanism that coordinates the generation of all three cell polarities? Or are these cell polarities inter-connected? These questions are currently little addressed. In this study, we show that the apical complex molecule aPKC is a key molecule to coordinate the formation of these three polarities and that one of the functions of Crumb complex, Par complex and the endocytic recycling machinery is to ensure a polarized distribution of aPKC at the inside apical junction and the outside lateral membrane respectively.

Results

Crb complex is required for front-back polarity of border cell clusters

Previous works have analyzed the roles of several apical and basolateral polarity components in border cells, including Par complex components Baz/Par3 and Par6, the adherens junction molecule E-cadherin (E-cad), and the lateral complex components Dlg and Lgl (Goode and Perrimon, 1997; Niewiadomska et al., 1999; Pinheiro and Montell, 2004; Szafranski and Goode, 2004). Here, we utilized both *in vivo RNAi* and genetic mosaics approaches to determine the functional roles of Crb complex. We found that loss of function of Crb complex components resulted in significant border cell migration defects. Expressing the *sdt* or *patj RNAi* in the border cells by a border cell specific *Gal4* driver (*slbo-Gal4*) caused significant migration delay when compared to the wild type control (Fig. 1B and Fig. S1A-B). The quantified migration index (MI) of control is close to 1 (0.96), and the MIs of *sdt* and *patj RNAi* are 0.79 and 0.83 respectively (Fig. 1B). Importantly, multiple stocks for *patj RNAi* (4) and *sdt RNAi* (3), which were obtained from different sources (see Materials and Methods), were tested and displayed similar migration delay (data not shown). Furthermore, staining of egg chambers containing Flip-out clones expressing *patj RNAi* with the Patj antibody revealed that Patj level was strongly reduced in the clones, indicating effective knockdown of *patj* function (Fig. S1C). Together, these results strongly support that the phenotypes of *patj RNAi* and *sdt RNAi* are indeed loss

of function of *patj* or *sdt* respectively. Generation of mosaic border cell clusters containing homozygous *crb*⁸²⁻⁰⁴ or *crb*^{1B5} mutant clones revealed more severe defects (MI=0.49, Fig. 1B and Fig. S1D; MI=0.68, Fig. S1E,F). Furthermore, *sdt* and *patj* RNAi in the heterozygous background of *sdt*^{K85}/+ (Krahn et al., 2010) and *Patj*^{Δ1}/+ (Sen et al., 2012) respectively resulted in more severe migration defects than the RNAi alone (MIs of 0.56 and 0.44 respectively; Fig. 1B). The results clearly indicate that the three Crumbs complex components are all required for border cell migration. Staining with the F-actin binding phalloidin dye revealed that those border cell clusters with migration delay typically displayed ectopic F-actin enriched patches on the side and back of the clusters (Fig. 1C,D and Fig. S1G), indicating a reduction of polarized F-actin distribution at the front. Moreover, mosaic clusters containing two wildtype polar cells and all *crb*⁸²⁻⁰⁴ border cells demonstrate that the phenotype of ectopic actin patches is autonomous to border cells (Fig. S2). Using a fast dissection method, we were able to better preserve the dynamic actin structures and found the actin patches to resemble lamellipodial protrusions (Fig. S3). Indeed, live imaging of stage 9 egg chambers confirmed the presence of ectopic dynamic protrusions at the side and back of the clusters, in addition to the leading protrusion at the front (Fig. 1E,F, Movies 1-3). It is known that a normal front-back polarity for border cell clusters involves confining a predominant protrusion to the leading cell and suppressing protrusions in the side cells. Together, our results demonstrate that loss-of-function of Crb complex components disrupts such a front-back polarity.

Patj and Sdt are required for positioning of apical-basal axis relative to the migration direction

Upon closer examination, we found that *Patj* or *Sdt*-deficient border cell clusters stained with the apical marker Baz exhibited a major defect in the positioning of the entire cluster with respect to the migration direction. In the wild type control, the border cell cluster was positioned in such a way that its apical-basal axis was always perpendicular to the migration direction (along the anterior-posterior axis) (Fig. 2A,B).

This is presumably due to the fact that the outer border cells, especially the leading cells, almost always (90% of the time) extended their protrusions at the lateral region of outer cortex (Fig. 2C-E) (Montell et al., 2012; Veeman and McDonald, 2016). However, migrating border cell clusters expressing *patj* or *sdt RNAi* were positioned such that their apical-basal axis was no longer at a 90-degree angle but at random angles to the anterior-posterior axis (Fig. 2A,B; data not shown). Furthermore, co-staining with Baz and phalloidin revealed that the ectopic protrusions mentioned above were distributed randomly in the top, middle and bottom sections of the outside membrane (Fig. 2C-E), which roughly correspond to the apical, lateral and basal regions respectively. This result indicates that loss of apical polarity molecules leads to loss of exclusive and lateral localization of lamellipodial protrusions and hence random positioning of the protrusions along apical-basal axis, which likely caused the apical-basal axis of entire border cell clusters to appear at random angles to the migration direction. Such positioning conceivably could lead to inefficient collective migration of the cluster. Together, these results demonstrate that Crb complex components Patj and Sdt are required for the polarized positioning of protrusions along the apical-basal axis.

Loss of front-back polarity is not due to lack of cell-cell communication

The phenotype of ectopic protrusions as resulted from loss of Crb complex components resembles border cells that are defective in cell-cell communication (Ramel et al., 2013; Wang et al., 2010). Previous reports have shown that border cell clusters deficient in JNK signaling displayed defects in cell adhesions between border cells and resulted in loss of cell-cell communication, which was revealed using a method involving photo-activation (PA) of Rac (Llense and Martin-Blanco, 2008; Wang et al., 2010). Border cells expressing a *PA-Rac* transgene can respond to blue laser light and activate the exogenous PA-Rac. When Rac was photo-activated in the lagging border cell, ectopic protrusion was induced by the active Rac in the back of cluster, and the leading border cell that is at least one cell distance away somehow

sensed the communication from the cells at the back and side of the cluster and retracted the leading protrusion within 30 minutes (Fig. S4A) (Wang et al., 2010). It was reported that in border cells where JNK signaling is down-regulated, cell-cell communication was abolished and ectopic protrusions formed in the back and side of the cluster (Wang et al., 2010), similar to clusters lacking the Crb complex components. It was previously proposed that the homotypic and transmembrane Crb might act in the apical junction between adjacent border cells to mediate cell-cell adhesion (Thompson et al., 2013). So, Crb complex could in theory mediate the non-autonomous communication between cells. However, we found that photo-activation of Rac in the back of *patj RNAi* border cell clusters resulted in induction of a new protrusion at the back, retraction of the leading and ectopic protrusions, and redirection of collective migration to the opposite direction (Fig. S4A-C). These results demonstrate that *patj RNAi* clusters possess normal cell-cell communication and that lack of cell-cell communication is not the cause for ectopic protrusions and disruption in front-back polarity.

Disruption in front-back and apical-basal polarities is due to mislocalized aPKC

To investigate what caused the disruption of front-back and apical-basal polarities in border cells lacking Crb complex components, we performed immunostaining for a variety of polarity and cytoskeletal markers. In the wild type border cell cluster, we found that Crb complex components such as Crb, Sdt and Patj and Par complex components such as Par6, aPKC and Baz were primarily localized in the apical junction between any two adjacent cells (Fig. 3A-F and Fig. S5), while a second pool of these molecules was distributed at moderate levels in the cytoplasm and near the outer cell periphery of each cell (Fig. 3A,B and Fig. S5). Furthermore, the second pool of the apical complex components displayed a front polarized distribution pattern and was often observed to be enriched in the leading protrusions (Fig. 3A-C and Fig. S6). However, loss of function of Sdt, Patj, or Crb caused disruption in the apical localization of the Crb complex and Par complex components except for Baz (Fig. 3A-F, Fig. S7A; data not shown), supporting the previous proposal that Crb complex

and Par complex together act as one super complex to regulate apical polarity and depletion of one complex affects the apical distribution of the other complex (Tepass, 2012; Thompson et al., 2013). It is important to note that *patj RNAi* caused strong disruption in the distribution of the Crb and Sdt in the apical junctions (Fig. 3E,F). This result indicates that Patj is required for the stability of Crb complex in the apical junctions, suggesting that it is indeed a functional component of Crb complex in border cells. Interestingly, Baz's distribution pattern in the apical junction was not grossly affected, consistent with previous finding that Baz functioned independently of the Par6-aPKC complex and was localized sub-apically below the aPKC apical domain in follicle cells (Morais-de-Sa et al., 2010). In addition, the sub-apical and lateral junctional distribution of E-cad and the lateral junctional distribution of Dlg was not grossly affected (Fig. 3E,F). Such loss of function of Crb complex components also resulted in increased distribution of Crb and Par complex components throughout the cytoplasm in the form of large ectopic dots (Fig. 3E,F). Among these components, we found that aPKC and Par6 displayed a unique ectopic distribution pattern, where they often colocalized with the aforementioned ectopic actin patches that were shown to be the ectopic protrusions (Fig. 3G,H and Fig. S9B). Furthermore, such colocalization is specific since large internal actin patches induced by reduction of cofilin (an actin depolymerizing factor) displayed no colocalization with ectopic aPKC spots (Fig. S7B). The unique association between ectopic protrusions and aPKC and Par6 spots suggested that ectopically localized aPKC and Par6 caused the extra protrusions. To test this idea, we reduced the function of aPKC or Par6 in the background of Patj loss-of-function, and found that aPKC but not Par6 loss-of-function rescued the phenotype of ectopic actin patches (Fig. 5A,B, Movie 4). Furthermore, knockdown of Par6 by itself still resulted in ectopic actin patches colocalizing with large aPKC spots (Fig. 3G,H), whereas knockdown or dominant negative inactivation of aPKC (aPKC-DN) resulted in a very different phenotype, which is virtual absence of non-leading protrusions or actin patches and reduced length of leading protrusions (Fig. 4A,B, Movie 5). Together, these results demonstrate that aPKC is required for protrusion formation in the wild type and that

mislocalized aPKC as resulted from loss of Crb complex components caused the formation of ectopic protrusions and disruption of front-back and apical-basal polarities.

This conclusion led to the possibility that aPKC is sufficient for formation of ectopic protrusions. To test this, we overexpressed wild type and active forms of aPKC including the membrane tethered aPKC-CAAX and the constitutively active aPKC-CA (with N-terminus deletion) in the border cells (Lee et al., 2006), and found large ectopic protrusions as well as increased F-actin levels present in these border cell clusters (Fig. 4B,C, Movie 5). Moreover, overexpressing active forms of aPKC in individual border cells within a cluster using the flip-out technique resulted in autonomous generation of large protrusions (Fig. 4D), demonstrating the autonomous protrusion-promoting ability of aPKC in individual border cells. Lastly, expressing the constitutively active aPKC-CA in single cell clones within an otherwise wild type cluster revealed that local or autonomous increase of aPKC activity in single cell caused that cell to behave much more like a leading cell as compared to single cell with only GFP expression (Fig. 4E).

Reduction of Crb complex or increased aPKC activity affected the inside-outside polarity

We found that overexpressing the active forms of aPKC (aPKC-CA and aPKC-CAAX) in border cells by *slbo-Gal4* caused reduction of cell-cell contact area between adjacent border cells and enlargement of membrane area contacting the substrate nurse cells, resulting in the appearance of every border cell outstretching away from the central polar cells (Fig. 4F, Movie 5). This result clearly shows a significant part of inside membrane (Fig. 3D), which normally displays strong cell adhesion and little membrane dynamics, has taken on the features of outside membrane (Fig. 3D), which typically displays high membrane and actin dynamics. As a result, the border cells do not behave as a coherent cluster undergoing collective migration, rather they act more

like cells migrating individually on their own even though they are held together by their adhesion to the central polar cells (Fig. 4F, Movie 5). This phenotype resembles the mutant phenotype of *crb*, in which individual border cells became more separated and ectopic actin patches formed between adjacent border cells (Fig. 1C, Fig. 4G,H). Indeed, in border cells with *Patj* and *Sdt* reduction, ectopic actin patches that were colocalized with aPKC not only formed in the outside cell cortex but were also observed to sometimes form in areas near cell-cell contacts (Fig. 3G,H). On the contrary, overexpressing *Crb* in the border cells resulted in much less actin-rich protrusions, little membrane dynamics and much reduced F-actin levels in the outside membrane (Fig. 4G,H), which appeared to take on the characteristics of inside membrane. Interestingly, reducing the aPKC activity also resulted in the similar phenotypes, which include much reduced front protrusions, no side and back protrusions and significantly reduced F-actin levels in the outside membrane (Fig. 4A,C,F,H). Taken together, these results suggest that *Crb* complex is required to maintain the inside-outside polarity probably by restricting aPKC's actin-promoting function to the outside membrane.

Ectopic protrusions were mediated by Sif and Rac

Rac and its positive regulators have been demonstrated to be critical for actin polymerization and protrusion formation in migratory cells including border cells (Heasman and Ridley, 2008; Montell, 2003; Montell et al., 2012). We then examined whether they mediated the generation of ectopic protrusions as a result of lack of *Crb* components. Using the similar genetic approach as mentioned above, we reduced the function of Rac in the background of *Patj* or *Sdt* loss-of-function (Fig. 5A,B; data not shown). We found that the ectopic actin patch phenotype was successfully rescued (Fig. 5A,B). Furthermore, using a previously reported Rac-FRET (Fluorescence Resonance Energy Transfer) sensor and live imaging (Wang et al., 2010), we observed that strong Rac activity was present in the ectopic protrusions (Fig. 5C-E), suggesting that increased Rac activity in the side and back of border cells was responsible for

ectopic protrusions. Previous studies reported that Vav and Mbc (myoblast city), both guanine exchange factors (GEFs) and hence positive regulators of Rac, were shown to promote protrusion formation and migration (Bianco et al., 2007; Duchek et al., 2001; Fernandez-Espartero et al., 2013). We then tested whether reducing the function of Vav and Mbc, as well as Sif, another Rac GEF and a *Drosophila* homolog of mammalian Tiam1 (Sone et al., 1997), could produce similar rescue as Rac. The results showed that knockdown of Sif but not of Vav or Mbc rescued the *patj RNAi* phenotype (Fig. 5A,B, Movie 4). Since individual knockdown of Sif, Vav or Mbc each caused reduced length of leading protrusion and migration delay of border cell cluster (Fig. S8), Sif's rescue effect on ectopic protrusions is specific. Together, these results demonstrate that Sif and Rac mediate the ectopic protrusions as resulted from lack of Patj.

aPKC acts through Sif to promote Rac activity and protrusions

It is previously known that Par complex interacts and activates mammalian Tiam1 and that aPKC was recently shown to interact with and phosphorylate Tiam1 in cultured mammalian cells (Chen and Macara, 2005; Matsuzawa et al., 2016; Wang et al., 2012; Zhang and Macara, 2006). We then tested whether aPKC could act through Sif to promote Rac activity and protrusions. First, we found that knockdown of Sif but not of Vav or Mbc in border cells could suppress the ectopic protrusions as resulted from overexpression of active aPKC (Fig. 6A,B, Movie 6). Moreover, Sif knockdown also suppressed the phenotypes of increased F-actin levels and delayed migration (Fig. 6B,C,D). In contrast, expression of dominant negative form of aPKC (aPKC-DN) failed to rescue the ectopic protrusion phenotype of Sif overexpression (Movie 7). Moreover, overexpressing Sif also mimicked the phenotypes of active aPKC overexpression (Fig. 6A,C, Movie 6). Together, these results indicate that aPKC acts genetically upstream of Sif. Second, dominant negative form of Rac (RacN17) could strongly suppress the phenotype of ectopic protrusions or increased F-actin levels as resulted from active aPKC or Sif overexpression respectively (Fig. 6C, E-G). And

overexpressing active aPKC resulted in marked increase of Rac activity as marked by the Rac-FRET sensor (Fig. 6H,I), which is similar to that resulted from *patj RNAi* (Fig. 5C,D). Third, co-immunoprecipitation (co-IP) experiments demonstrated that Myc-tagged Sif (Myc-Sif) physically interacted with aPKC-GFP (Fig. 6J).

Lastly, we generated a transgene encoding HA-tagged Sif (HA-Sif) to determine its localization pattern in border cells (Fig. 6K,L). Staining with HA antibody revealed that HA-Sif was localized both in cytoplasm and near membrane, with a polarized distribution toward the front in the leading cells (Fig 6K). Interestingly, most of the HA-Sif staining was localized in the basolateral region of border cell clusters, whereas the predominant population of membrane-bound aPKC is localized in the apical junctions, a region that is spatially segregated from HA-Sif's localization (Fig. 6L, 2nd and 3rd rows). However, the non-apical population of aPKC near the outside membrane at the basolateral position displayed significant overlap with HA-Sif (Fig. 6L, 1st row). This result suggests that aPKC that is localized in apical junctions could not interact with Sif strongly in the apical region due to lower level of Sif available there. But Sif's overlap with the non-apical aPKC pool near the outside lateral membrane could promote the formation of protrusion there. Lastly, co-expression of HA-Sif and aPKC-GFP in *Drosophila* S2 cells showed that HA-Sif partially colocalized with aPKC-GFP in both cell membrane and in cytoplasm (Fig. 6M). Taken together, our results indicate that aPKC interacts with and acts through Sif near the outside membrane at basolateral region to promote Rac activity and actin-based protrusions.

Endocytic recycling is required for the polarized distribution of two distinct pools of apical complex components

Immunostaining revealed that Crb complex components and Par complex components each displayed distribution of two distinct populations (Fig. 3A-C). The major pool resided in the apical junctions, whereas the minor pool was present close to the outside and lateral cell membrane of border cells. Interestingly, some components such as aPKC, Patj and Crb even displayed a front-back asymmetry for the second minor pool (Fig. 3C), and the front polarized distribution of aPKC requires the function of the guidance receptor PVR (Fig. 7A,B). Live imaging also revealed that punctate spots of Par6-GFP (a genomic transgene driven by the *par6* promoter), which is mostly enriched in the apical junction, could be found trafficking from apical junction to the outside membrane, suggesting that there may be dynamic exchange between the two pools (Fig. S9A). We then attempted to decipher the mechanism behind distribution of two distinct pools of apical components. Previous studies from our and other labs have shown that endocytic recycling machinery is required for front-back polarity and collective migration of border cell clusters (Assaker et al., 2010; Jekely et al., 2005; Laflamme et al., 2012; Wan et al., 2013). We then tested whether vesicle trafficking could be the means to generate the polarized distribution of these two pools. Interestingly, we found that loss of function of the endocytic regulators dynamin and Rab5, the recycling regulator Rab11, and the exocytosis regulator Sec3 each resulted in severe disruption in the distribution of and balance between the two pools of apical polarity molecules (Fig. 7C-H). For instance, reduction of Rab11 or Sec3 caused dramatic disruption of Crb and aPKC at the apical junction, accompanied by strong increase of their staining in the cytoplasm (Fig. 7C-F). Loss of function of Rab5 or dynamin (encoded by *shi*) resulted in a strong sharp line of membrane staining of Crb and aPKC or Baz and aPKC respectively at the outside lateral membrane (Fig. 7G,H), which is very different from their diffused staining pattern near the outside membrane of wild type border cells (Fig. 7G,H and

Fig. 3A-C). Moreover, their apical junction localization pattern was also disrupted and their cytoplasmic stainings were increased. This result suggests that in the wild type border cells, membrane-bound apical polarity molecules at the outside membrane need to be constantly trafficked to the cytoplasm by dynamin and Rab5-mediated endocytosis. Together, these results demonstrate that the endocytic recycling machinery is required for the polarized distribution of two distinct pools of apical polarity proteins, but whether localization of these polarity molecules were directly or indirectly regulated by endocytic recycling is not clear.

On the other hand, we then sought to determine whether polarized recycling and exocytosis were affected by Crb complex disruption. Our previous work indicated that Rab11-labeled recycling endosomes and Sec5-labeled exocysts displayed a front-polarized distribution near the leading protrusion, which depends on signaling from the guidance receptor PVR (Wan et al., 2013). But in *patj RNAi* border cell clusters (where Crb complex was disrupted; Fig. 3E,F), Rab11 and Sec5 stainings were shown to be enriched in the ectopic protrusions, with no apparent polarized distribution at the front of clusters (Fig. 7I,J,M), implying that the locally enriched recycling endosomes and exocysts were somehow involved in mis-trafficking of aPKC and hence formation of ectopic protrusions (Fig. 7M). Indeed, locally enriched Rab11 staining was shown to partially colocalize with large and ectopically localized aPKC spots in *patj RNAi* border cell clusters (Fig. S10). And reducing the function of Rab11 effectively suppressed the formation of ectopic actin patches or protrusions as resulted from *patj RNAi* (Fig. 7K,L). Together, these results demonstrate that disruption of Crb complex also affects the distribution pattern of recycling endosome and exocyst and that redistribution of aPKC likely depends on recycling endosome.

Discussion

This study demonstrates that Crb complex is required for collective migration of border cells. Loss of function of Crb, Sdt or Patj each delayed the border cell migration, likely as a result of the combined effect of disrupting three distinct cell polarities (Fig. 7M). Most importantly, the front-back polarity of the border cell cluster is disrupted, as demonstrated in the ectopic formation of large actin-rich protrusions in border cells located at the side and back of cluster (Fig. 7M). Furthermore, *patj* or *sdt RNAi* caused border cell clusters to extend major protrusions at random angles to the apical-basal axis, unlike the wild type clusters that restrict the protrusion formation only to the lateral region, thus extending the protrusion perpendicular to their inherent apical-basal axis (Fig. 7M). Such restriction of lateral protrusion formation would ensure the protrusion to be parallel to the migration direction, resulting in efficient forward movement of the entire cluster. Lastly, mutation in *crb* or expression of active form of aPKC expands the outside membrane area, and overexpression of Crb or reducing aPKC activity suppresses the outside membrane characteristics, causing disruption in inside-outside polarity for each border cell. Interestingly, *crb* mutant border cells sometimes exhibited ectopic actin patches (containing large aPKC spots) between the adjacent cells (Fig. 7M), where inside membrane is normally located. Taken together, these results raise the following question: is there a common mechanism that is affected during the disruption of all three cell polarities? In other words, are these cell polarities inter-connected and coordinated by a common mechanism?

Interestingly, we found that a common feature of loss of Crb complex components is that mislocalized aPKC generates ectopic Rac-dependent protrusions in border cells at side and back of cluster and at the apical and inside (junctional) region of individual border cells, leading to disruption of all three cell polarities. This indicates that there is a common mechanism involving aPKC that organizes all three polarities. First, the

ectopic protrusions and loss of these three polarities as a result of loss of Patj is likely mediated by the ectopically localized aPKC since reduction of aPKC could rescue the ectopic protrusions. Interestingly, loss of other apical polarity proteins (Crb, Sdt, Par6, Cdc42) except for aPKC and Baz also led to similar phenotypes, including disrupted aPKC localization in the apical junctions, ectopic actin patches colocalized with large aPKC spots, and increased F-actin levels and Rac activity at or near the outside membrane. In contrast, loss of aPKC resulted in few protrusions and reduced F-actin levels at outside membrane, while overactivation of aPKC led to increased F-actin levels and Rac activity, which are mediated by the downstream Sif/TIAM1. These results suggest that an important role of the Crb and Par complexes is through sequestering most of aPKC in the apical junction, leaving only moderate level of aPKC near outside membrane to promote protrusions. The major pool of aPKC at the apical junction (together with Crb and Par complex components) likely functions similar to its classical role in epithelial cells, which is to promote apical polarity and integrity of apical and sub-apical junctions. But the minor aPKC pool near outside lateral membrane may function differently in that it can activate Sif to increase Rac-mediated actin dynamics. Such difference may arise from the possible scenario that the apical complexes at the apical junction restrict or inhibit aPKC's Sif-promoting activity. Conceivably, such inhibition would not apply to aPKC near the outside lateral membrane.

As summarized by our model diagram (Fig. 7M), a critical function of Crumb complex and Par complex is to cause a high level of membrane-bound aPKC at the inside apical junction and a moderate level of cytoplasmic aPKC near the outside lateral membrane so that the three distinct but related cell polarities could be properly established. Furthermore, polarized endocytic recycling of vesicles associated with aPKC and other apical polarity molecules ensures the polarized distribution of two aPKC pools within each border cell. Finally, it is interesting to note that the front-polarized recycling and exocytosis within the WT cluster as mediated by PVF-PVR guidance signaling (Wan et al., 2013) could cause aPKC to be much more

enriched at the outside membrane of leading edge (to promote leading protrusion) than at the outside membrane at the side and back of border cell cluster (to promote minor side protrusions). When cells migrate collectively under developmental, physiological and pathological contexts, the migrating sheets or clusters of cells often display part-epithelial and part-mesenchymal characteristics. It will be interesting to determine whether aPKC together with Crb and Par complexes and endocytic recycling machinery also play conserved roles in coordinating these three cell polarities in other types of collective migration.

Materials and Methods

Drosophila genetics

Flies were cultured following standard procedures at 25 °C except for RNAi experiment (at 29 °C). All strains were obtained from the Bloomington *Drosophila* Stock Center, National Institute of Genetics Stock Center (Japan), Vienna *Drosophila* RNAi Center, and Tsinghua University RNAi Stock Center, except for the followings: *crb*⁸²⁻⁰⁴ (Ling et al., 2010), *patj*^{Δ7} (Zhou and Hong, 2012), *DEcad::GFP* (Huang et al., 2009), *Crb-HA* (Huang et al., 2009), *patj*^{Δ1} (Sen et al., 2012), *sdt*^{K85} (Krahn et al., 2010), *UAS-aPKC-CAAX* (Lee et al., 2006), *UAS-aPKC-DN* (Lee et al., 2006), *UAS-aPKC-CA* (Lee et al., 2006), *UAS-aPKC* (Lee et al., 2006), *sec3*^{PBac} (Wan et al., 2013), *UAS-RacFRET* (Wang et al., 2010), *UAS-PARacQ61L* (Wang et al., 2010), *UAS-PARacQ61L-C450M* (Wang et al., 2010). To generate *UAS-HA-sif* transgenic line, a full-length cDNA of *sif* gene was obtained and amplified from the genome of the *UAS-sif* fly stock (stock# 9127, BDSC), then the PCR product was fully sequenced and subcloned into pUAST-HA vector. HA fragment was localized at the N terminus of the Sif protein. Then the recombined vector was injected into embryos according to standard procedures. The primers for *HA-sif* are as follows:

sif-F1:5'-AGCGCGTTACCACATAGATCTATGGGTAACAACTGAGCTGC-3',

sif-R1:5'-TCCTCTAGAGGTACCCTCGAGCTTAATTTTTCACATCGTCTTTGC-3'.

FRT clone was induced by *hs-FLP*. Heat shock was applied starting from late 3rd instar larval or early pupal stage at 37°C for 2 hours per day for 3 days. After eclosion, flies were raised on yeast supplemented media for 2 days before dissection. To perform flip-out experiments, *AyGal4 UAS-transgenes* were crossed to *hs-Flp*. Newly enclosed flies were heat shocked in 37°C water bath for 5 minutes. For analysis of single cell clones, mosaic clusters with only one border cell expressing GFP were used. Flies obtained from the public stock centers are listed in the table below.

GENOTYPE	STOCK #	USE FREQUENCY	SOURCE
<i>UAS-patj.RNAi</i>	THU1704	++	Tsinghua University RNAi Stock Center (TURSC)
<i>UAS-patj.RNAi</i>	12021R-3	+	National Institute of Genetics (NIG)
<i>UAS-patj.RNAi</i>	31620	+	Vienna Drosophila Research Center (VDRC)
<i>UAS-patj.RNAi</i>	101877	+	VDRC
<i>UAS-sdt.RNAi</i>	THU1336	++	TURSC
<i>UAS-sdt.RNAi</i>	29844	+	VDRC
<i>UAS-sdt.RNAi</i>	15342R-2	+	NIG
<i>UAS-aPKC.RNAi</i>	THU5841	++	TURSC
<i>UAS-aPKC.RNAi</i>	105624	++	VDRC
<i>UAS-baz.RNAi</i>	5055R-1	++	NIG
<i>UAS-baz.RNAi</i>	5055R-2	++	NIG
<i>UAS-baz.RNAi</i>	2915	+	VDRC
<i>UAS-baz.RNAi</i>	2914	++	VDRC
<i>UAS-par6.RNAi</i>	19731	+	VDRC
<i>UAS-par6.RNAi</i>	THU3865	++	TURSC
<i>UAS-sif.RNAi</i>	5406R-2	++	NIG
<i>UAS-sif.RNAi</i>	5406R-3	++	NIG
<i>UAS-sif.RNAi</i>	25789	+	Bloomington Drosophila Stock Center (BDSC)
<i>UAS-vav.RNAi</i>	6241	++	VDRC
<i>UAS-mbc.RNAi</i>	TH02182.N	+	TURSC
<i>UAS-mbc.RNAi</i>	TH02150.N	++	TURSC
<i>UAS-mbc.RNAi</i>	THU0808	++	TURSC
<i>UAS-mbc.RNAi</i>	TH01095.N2	+	TURSC
<i>UAS-cdc42.RNAi</i>	12530R-2	++	NIG
<i>UAS-cdc42.RNAi</i>	12530R-3	++	NIG

<i>UAS-cdc42.RNAi</i>	29004	+	BDSC
<i>UAS-crb</i>	5544		BDSC
<i>UAS-Rab5-DN</i>	9771		BDSC
<i>UAS-Rab11-DN</i>	23261		BDSC
<i>UAS-Shi-DN</i>	108437		KYOTO Stock Center (DGRC)
<i>UAS-Shi-DN</i>	108445		DGRC
<i>UAS-clc.GFP</i>	7107		BDSC
<i>UAS-sif</i>	9127		BDSC
<i>FRT82B</i> <i>crb[j1B5]/TM6B</i>	111051		DGRC
<i>UAS-GFP</i>	1522		BDSC
<i>UAS-RacN17</i>	6292		BDSC
<i>UAS-patj</i>	39735		BDSC
<i>UAS-tsrl.RNAi</i>	110599		VDRC
<i>UAS-Lifeact.Ruby</i>	35545		BDSC
<i>UAS-Lifeact.GFP</i>	35544		BDSC

++ RNAi stocks more frequently used in this study.

+ RNAi stocks sometimes used in this study.

Immunostaining and microscopy

Ovary dissection was carried out in phosphate-buffered saline (PBS) and then fixed in devitellinizing buffer (7% formaldehyde) and heptane (Sigma) mixture (1:6) for 10 minutes (Zhang et al., 2011). After 3 times washes in PBS, ovaries were incubated in PBT (PBS+3% triton X-100) and blocking solution (PBT, 10% goat serum) for 30min and then stained overnight at 4 °C. The difference between fast dissection and normal dissection is that the time of fast dissection was less than 5 minutes and involved fewer ovaries than normal dissection method, which typically took about 20 minutes. Primary antibodies and their concentrations were as follows: mouse anti-phospho-Tyr (4G10, 1:200, Millipore), mouse anti-Rab11 (1:200, BD transduction), mouse anti-Enable (5G2, 1:100, Developmental Studies Hybridoma Bank (DSHB)), rat anti-E-cad (DCAD2, 1:50, DSHB), goat-anti-Arp2 (sc-11968, 1:10, Santa Cruz), mouse anti-Dlg (4F3, 1:100, DSHB), mouse anti-Crb (Cq4, 1:10, DSHB), mouse-anti-Armdillo (N2 7A1, 1:50, DSHB), rabbit anti-PKC ζ (C-20, 1:200, Santa Cruz), rabbit anti-p-Myosin II (3671S, 1:100, Cell Signaling), rat anti-HA (3F10, 1:100, Roche), rabbit anti-Baz (1:400, gift from A. Wodarz), mouse anti-Sec5 (1:50,

gift from T. Schwarz), mouse anti-Patj (1:800, gift from Hong Yang), rabbit anti-Sdt (1:500, gift from E. Knust). Methanol treatment was used before anti-Crb staining as described previously (Niewiadomska et al., 1999). After washes in PBT, ovaries were incubated with secondary antibodies (1:200, Jackson ImmunoResearch) for 2 hours at room temperature. F-actin was labeled by Rhodamine phalloidin (1:200, Sigma). Confocal images were obtained using a Leica TCS SP5 II, an Olympus FV1200, or a Zeiss 880 microscope (with Airyscan technology) and images were processed by Image J, Imaris (Bitplane) and MATLAB softwares.

Live imaging and photomanipulation

Egg chambers were dissected from ovaries and mounted for live imaging as described previously (Prasad et al., 2007). Rac FRET imaging and analysis were done as described by Wang et al. (Wang et al., 2010). CFP and YFP images were acquired by the Zeiss 880 confocal microscope and processed by Image J. A Gaussian smooth filter was applied to both channels, with background subtracted. CFP image was then used to create a binary mask with the background set to zero. The final ratio images were generated from YFP/CFP ratios. The FRET index was calculated in the entire border cell cluster by measuring the average intensity of FRET. Heat maps of FRET indices were generated with MATLAB. Rac photoactivation was performed as described previously by Wang et al. (Wang et al., 2010). To photoactivate, the 458nm laser was set at 8% laser power and illuminated in a 7µm diameter spot. The photoactivation scan lasted about 30s. The border cells were then imaged using 568nm laser. This series of steps was repeated for the duration of the time lapse experiment. Live imaging of Lifeact-GFP was carried out using Leica SP11 confocal microscope equipped with a HyD detector. Live imaging of Par6-GFP was performed by Olympus FV1200 with a GaAsP detector.

Quantification of border cell migration

Border cells were labeled by expression of *UAS-GFP* using *slbo-GAL4* driver. To quantify border cell migration, stage 10 egg chambers were used. Depending on the positioning of the cluster along the migratory route (between anterior tip of egg chamber and oocyte border), the extent of border cell migration was measured and categorized into 5 classes, which are 0% (no migration), 25%, 50%, 75% and 100% (arriving at border) respectively. Migration Index (M.I.) was then calculated according to the following formula to evaluate migratory ability, as described previously (Assaker et al., 2010):

$$M.I. = \frac{1 \cdot n(100\%) + 0.75 \cdot n(75\%) + 0.5 \cdot n(50\%) + 0.25 \cdot n(25\%) + 0 \cdot n(0\%) + 0.5 \cdot n(dis)}{N}$$

For example, $n(75\%)$ represents the number of stage 10 egg chambers in which border cell clusters were found at 75% of migration distance. $n(dis)$ represents the number of border cell clusters that were disassociated and not coherent. Disassociated clusters were very rare in our experiments. N is the total number of stage 10 egg chambers examined.

Measurement of protrusions

For fixed samples, a z-series of confocal sections was taken for each border cell cluster. After going through the z-series, the confocal section with the longest protrusion visible was selected and measurement was performed for the protrusion. For the phalloidin-labeled protrusions, the length of protrusion was determined by the distance from the tip of protrusion to the boundary between basal region of protrusion (enriched with phalloidin staining) and cell body (much less phalloidin staining), as described previously (Zhang et al., 2011). Protrusions that are longer than 2 μm and with significant width were qualified as protrusions and used for calculation. To determine the distribution of actin patches or protrusions, border cell clusters were divided into four quadrants: 1 front quadrant, 2 middle and 1 back quadrants.

Protrusions extended from the front quadrant were defined as leading protrusions, protrusions extended from other regions were considered non-leading protrusions. To determine position of actin patches or protrusions along the apical-basal axis, Baz staining was used to label the apical side of border cell cluster. Confocal z-stacks of border cell clusters were acquired and processed by Imaris for 3-D reconstruction, from which protrusion position along apical-basal axis was determined.

For live imaging, Lifeact-GFP was used to label actin-enriched protrusions (Riedl et al., 2008). A z-series of about 25 confocal sections was taken every 2 minutes for each border cell cluster, and these confocal images were subjected to maximum projection. The length of the protrusions was measured and determined from the final projected image. Protrusions with at least 3 μm in length (from base to tip) and 3 μm in width at the base were counted. The extension lifetime of protrusions was determined from the onset of extension to the final moment of disappearance (complete retraction). The full 2-minute interval time would be included if the protrusion disappeared during the interval.

Definition of ectopic protrusions and ectopic actin patches

For ectopic protrusion (EP), a protrusion has to be at least 3 μm in length (from base to tip) and 3 μm in width at the base, according to the Lifeact-GFP labeling. Protrusions extended from side or back positions will be counted as EPs. When we see two or more protrusions situated at similar positions around the front of cluster, the larger one will be designated leading protrusion (LP). If two protrusions are similar in size and one is situated more toward the front or leading position, we will designate that protrusion the LP.

The “ectopic actin patches” are large and intense phalloidin-stained patches that are at least $4\mu\text{m}^2$ in area (measured by Image J). We do not count leading lamellipodial protrusions that contain fine actin-structures (with elongated lamellipodial shape) in the wild type and mutant clusters as “ectopic actin patches” for quantification purposes.

Analysis of border cell cluster position

To determine the alignment of entire border cell cluster with respect to the anterior-posterior axis of the egg chamber, Baz staining was used to label its apical side. A z-series of confocal sections was taken for each cluster with 0.4um between successive sections. The images were then reconstructed and analyzed in Imaris. The reconstructed images would be rotated along the anterior-posterior axis to facilitate the measurement of the angle between apical-basal axis of border cell and anterior-posterior axis.

Analysis of mosaic *crb* mutant clusters

For Fig. 1B, all 19 mosaic clusters that we used are mutant (homozygous *crb*⁸²⁻⁰⁴) for all the outer border cells, and 14/19 or 74% of mutant clusters demonstrate various degrees of migration delay (Fig. S1D). However, migration defects could also be observed when mosaic clusters contained clones of 2 or more mutant border cells (data not shown).

Quantification of fluorescence intensity

To measure fluorescence intensity of phalloidin staining, *w*¹¹¹⁸ (considered as wild type) egg chambers without GFP label were mixed with control or other genotypes that were labeled with GFP in the same vial for phalloidin staining. Average fluorescence intensity (FI) of *w*¹¹¹⁸ border cell clusters and FI of genotype of choice was each measured by Image J, and the normalized FI was determined by FI (genotype) / FI (*w*¹¹¹⁸).

To measure the front/back ratios for Fig. 3A,C, Fig. 6K and Fig. 7A,B, an area around the leading edge of the cluster was chosen as the front region, and an area including the lagging end was chosen as the back region. Average fluorescence intensity (FI) was measured by ImageJ software (NIH) for each region; the front/back ratios were calculated as [front FI] divided by [back FI]. *slbo-Gal4;UAS-GFP* was chosen as GFP controls for Fig. 3A,C and Fig. 6K, and it showed no front/back bias as its front/back ratio is approximately 1.

Immunoprecipitation assay

Drosophila S2 cells were transfected with *UAS-Myc-sif*, *UAS-aPKC-GFP*, or both, and their cell lysates were used for the immunoprecipitation assay. To generate *UAS-Myc-sif* construct, a full-length cDNA of the *sif* gene was amplified from the genome of the *UAS-sif* fly stock (stock# 9127, BDSC), then the PCR product was fully sequenced and cloned into pUAST-Myc vector. Myc fragment was localized at the N terminus of the Sif protein. The primers for *Myc-sif*:

sif-F2: 5'-GAGCAGATCTGCGGCCGCGGCATGGGTAAACAACTGAGCTGC-3',

sif-R2: 5'-CCTTCACAAAGATCCTCTAGTTAATTTTTCACATCGTCTTTGC-3'. To

generate the *UAS-aPKC-GFP* construct, the full length cDNA of aPKC was amplified from the FI03288 clone (*Drosophila* Genomics Resource Center (DGRC)) and then subcloned into pUAST vector. Coding sequence of GFP was inserted into the C terminal end of aPKC. The primers for *aPKC-GFP*:

aPKC-F: 5'-CGGAATTCATGCAGAAAATGCCCTCGCA-3'

aPKC-R: 5'-ACAGAGACCTCCTAACGCAGTCTAGAAG-3'

GFP-F: 5'- TGGGAATTCGTTAACAGATCTATGGTGAGCAAGGGCGAGGA-3'

GFP-R: 5'- TCCTCTAGAGGTACCCTCGAGTTACTTGTACAGCTCGTCCATGC-3'

S2 cell lysates were analyzed by immunoblotting with following primary antibodies: rabbit anti-GFP (FL,1:500, Santa Cruz), mouse anti-c-Myc (9E10, 1:500, Santa Cruz), rabbit anti-PKC ζ (C-20,1:500, Santa Cruz). Secondary antibody used was HRP-conjugated (Vazyme). For the immunoprecipitation, lysates were incubated with

5ml primary antibodies for overnight at 4°C, 50% protein A/G agarose beads (Protein A/G PLUS-Agarose, Santa Cruz) working solution (in PBS) was added to lysate and rocked for 4 h at 4°C. Lysates and immunoprecipitates were then immunoblotted.

Statistical analysis

Statistical analyses were performed with GraphPad Prism, version 5.01. Statistical comparisons of means were made using the unpaired student's two-tailed t-test. $P < 0.05$ was used as the criterion for statistical significance.

Competing interests

The authors declare no competing financial interests.

Acknowledgements

We thank Yang Hong for fly stocks and critical reading of the manuscript, Michael P. Krahn, Shian Wu, Cheng-yu Lee, Bloomington Drosophila Stock Center, Tsinghua University RNAi Stock Center, National Institute of Genetics Stock Center (Japan), and Vienna Drosophila RNAi Center for various fly stocks.

Funding

This work is supported by grants from National Natural Sciences Foundation of China (31171335, 31271488, 31071219) and Ministry of Science and Technology (2015BAI09B03) to J.C, and grant from the Institut National de la Santé et de la Recherche Médicale [the ATIP-Avenir program (2012–2016)] to X.W.

Author Contributions

Conceptualization, J.C., H.W., and X.W.; Methodology, J.C., H.W., and X.W.; Investigation, H.W., Z.Q., Z.X., S.J.C., J.L. and X.W.; Writing, J.C., H.W., and X.W.; Supervision, J.C. and X.W.

References

- Assaker, G., Ramel, D., Wculek, S. K., Gonzalez-Gaitan, M. and Emery, G. (2010). Spatial restriction of receptor tyrosine kinase activity through a polarized endocytic cycle controls border cell migration. *Proceedings of the National Academy of Sciences of the United States of America* **107**, 22558-22563.
- Bianco, A., Poukkula, M., Cliffe, A., Mathieu, J., Luque, C. M., Fulga, T. A. and Rorth, P. (2007). Two distinct modes of guidance signalling during collective migration of border cells. *Nature* **448**, 362-365.
- Cai, D., Chen, S. C., Prasad, M., He, L., Wang, X., Choessel-Cadamuro, V., Sawyer, J. K., Danuser, G. and Montell, D. J. (2014). Mechanical feedback through E-cadherin promotes direction sensing during collective cell migration. *Cell* **157**, 1146-1159.
- Chen, X. and Macara, I. G. (2005). Par-3 controls tight junction assembly through the Rac exchange factor Tiam1. *Nat Cell Biol* **7**, 262-269.
- Combedazou, A., Choessel-Cadamuro, V., Gay, G., Liu, J., Dupre, L., Ramel, D. and Wang, X. (2017). Myosin II governs collective cell migration behaviour downstream of guidance receptor signalling. *J Cell Sci* **130**, 97-103.
- Duchek, P., Somogyi, K., Jekely, G., Beccari, S. and Rorth, P. (2001). Guidance of cell migration by the Drosophila PDGF/VEGF receptor. *Cell* **107**, 17-26.
- Felix, M., Chayengia, M., Ghosh, R., Sharma, A. and Prasad, M. (2015). Pak3 regulates apical-basal polarity in migrating border cells during Drosophila oogenesis. *Development* **142**, 3692-3703.
- Fernandez-Espartero, C. H., Ramel, D., Farago, M., Malartre, M., Luque, C. M., Limanovich, S., Katzav, S., Emery, G. and Martin-Bermudo, M. D. (2013). GTP exchange factor Vav regulates guided cell migration by coupling guidance receptor signalling to local Rac activation. *J Cell Sci* **126**, 2285-2293.
- Friedl, P. and Gilmour, D. (2009). Collective cell migration in morphogenesis, regeneration and cancer. *Nature reviews. Molecular cell biology* **10**, 445-457.
- Goode, S. and Perrimon, N. (1997). Inhibition of patterned cell shape change and cell invasion by Discs large during Drosophila oogenesis. *Genes & development* **11**, 2532-2544.
- Heasman, S. J. and Ridley, A. J. (2008). Mammalian Rho GTPases: new insights into their functions from in vivo studies. *Nature reviews. Molecular cell biology* **9**, 690-701.
- Huang, J., Zhou, W., Dong, W., Watson, A. M. and Hong, Y. (2009). From the Cover: Directed, efficient, and versatile modifications of the Drosophila genome by genomic engineering. *Proceedings of the National Academy of Sciences of the United States of America* **106**, 8284-8289.
- Jekely, G., Sung, H. H., Luque, C. M. and Rorth, P. (2005). Regulators of endocytosis maintain localized receptor tyrosine kinase signaling in guided migration. *Dev Cell* **9**, 197-207.
- Knust, E. and Bossinger, O. (2002). Composition and formation of intercellular junctions in epithelial cells. *Science* **298**, 1955-1959.
- Krahn, M. P., Buckers, J., Kastrup, L. and Wodarz, A. (2010). Formation of a Bazooka-Stardust complex is essential for plasma membrane polarity in epithelia. *The Journal of cell biology* **190**, 751-760.
- Laflamme, C., Assaker, G., Ramel, D., Dorn, J. F., She, D., Maddox, P. S. and Emery, G. (2012). Evi5 promotes collective cell migration through its Rab-GAP activity. *J Cell Biol* **198**, 57-67.

- Lee, C. Y., Robinson, K. J. and Doe, C. Q. (2006). Lgl, Pins and aPKC regulate neuroblast self-renewal versus differentiation. *Nature* **439**, 594-598.
- Ling, C., Zheng, Y., Yin, F., Yu, J., Huang, J., Hong, Y., Wu, S. and Pan, D. (2010). The apical transmembrane protein Crumbs functions as a tumor suppressor that regulates Hippo signaling by binding to Expanded. *Proceedings of the National Academy of Sciences of the United States of America* **107**, 10532-10537.
- Llense, F. and Martin-Blanco, E. (2008). JNK signaling controls border cell cluster integrity and collective cell migration. *Current biology : CB* **18**, 538-544.
- Lucas, E. P., Khanal, I., Gaspar, P., Fletcher, G. C., Polesello, C., Tapon, N. and Thompson, B. J. (2013). The Hippo pathway polarizes the actin cytoskeleton during collective migration of Drosophila border cells. *The Journal of cell biology* **201**, 875-885.
- Matsuzawa, K., Akita, H., Watanabe, T., Kakeno, M., Matsui, T., Wang, S. and Kaibuchi, K. (2016). PAR3-aPKC regulates Tiam1 by modulating suppressive internal interactions. *Mol Biol Cell* **27**, 1511-1523.
- Montell, D. J. (2003). Border-cell migration: the race is on. *Nat Rev Mol Cell Biol* **4**, 13-24.
- Montell, D. J., Yoon, W. H. and Starz-Gaiano, M. (2012). Group choreography: mechanisms orchestrating the collective movement of border cells. *Nature reviews. Molecular cell biology* **13**, 631-645.
- Morais-de-Sa, E., Mirouse, V. and St Johnston, D. (2010). aPKC phosphorylation of Bazooka defines the apical/lateral border in Drosophila epithelial cells. *Cell* **141**, 509-523.
- Niewiadomska, P., Godt, D. and Tepass, U. (1999). DE-Cadherin is required for intercellular motility during Drosophila oogenesis. *The Journal of cell biology* **144**, 533-547.
- Penalva, C. and Mirouse, V. (2012). Tissue-specific function of Patj in regulating the Crumbs complex and epithelial polarity. *Development* **139**, 4549-4554.
- Pinheiro, E. M. and Montell, D. J. (2004). Requirement for Par-6 and Bazooka in Drosophila border cell migration. *Development* **131**, 5243-5251.
- Pocha, S. M. and Knust, E. (2013). Complexities of Crumbs function and regulation in tissue morphogenesis. *Current biology : CB* **23**, R289-293.
- Prasad, M., Jang, A. C., Starz-Gaiano, M., Melani, M. and Montell, D. J. (2007). A protocol for culturing Drosophila melanogaster stage 9 egg chambers for live imaging. *Nat Protoc* **2**, 2467-2473.
- Ramel, D., Wang, X., Laflamme, C., Montell, D. J. and Emery, G. (2013). Rab11 regulates cell-cell communication during collective cell movements. *Nat Cell Biol* **15**, 317-324.
- Riedl, J., Crevenna, A. H., Kessenbrock, K., Yu, J. H., Neukirchen, D., Bista, M., Bradke, F., Jenne, D., Holak, T. A., Werb, Z., et al. (2008). Lifeact: a versatile marker to visualize F-actin. *Nat Methods* **5**, 605-607.
- Sen, A., Nagy-Zsver-Vadas, Z. and Krahn, M. P. (2012). Drosophila PATJ supports adherens junction stability by modulating Myosin light chain activity. *The Journal of cell biology* **199**, 685-698.
- Sone, M., Hoshino, M., Suzuki, E., Kuroda, S., Kaibuchi, K., Nakagoshi, H., Saigo, K., Nabeshima, Y. and Hama, C. (1997). Still life, a protein in synaptic terminals of Drosophila homologous to GDP-GTP exchangers. *Science* **275**, 543-547.
- St Johnston, D. and Ahringer, J. (2010). Cell polarity in eggs and epithelia: parallels and diversity. *Cell* **141**, 757-774.
- Szafranski, P. and Goode, S. (2004). A Fasciclin 2 morphogenetic switch organizes epithelial cell cluster

- polarity and motility. *Development* **131**, 2023-2036.
- Tepass, U.** (2012). The apical polarity protein network in *Drosophila* epithelial cells: regulation of polarity, junctions, morphogenesis, cell growth, and survival. *Annu Rev Cell Dev Biol* **28**, 655-685.
- Thompson, B. J., Pichaud, F. and Roper, K.** (2013). Sticking together the Crumbs - an unexpected function for an old friend. *Nature reviews. Molecular cell biology* **14**, 307-314.
- Veeman, M. T. and McDonald, J. A.** (2016). Dynamics of cell polarity in tissue morphogenesis: a comparative view from *Drosophila* and *Ciona*. *F1000Res* **5**.
- Wan, P., Wang, D., Luo, J., Chu, D., Wang, H., Zhang, L. and Chen, J.** (2013). Guidance receptor promotes the asymmetric distribution of exocyst and recycling endosome during collective cell migration. *Development* **140**, 4797-4806.
- Wang, S., Watanabe, T., Matsuzawa, K., Katsumi, A., Kakeno, M., Matsui, T., Ye, F., Sato, K., Murase, K., Sugiyama, I., et al.** (2012). Tiam1 interaction with the PAR complex promotes talin-mediated Rac1 activation during polarized cell migration. *The Journal of cell biology* **199**, 331-345.
- Wang, X., He, L., Wu, Y. I., Hahn, K. M. and Montell, D. J.** (2010). Light-mediated activation reveals a key role for Rac in collective guidance of cell movement in vivo. *Nat Cell Biol* **12**, 591-597.
- Zhang, H. and Macara, I. G.** (2006). The polarity protein PAR-3 and TIAM1 cooperate in dendritic spine morphogenesis. *Nat Cell Biol* **8**, 227-237.
- Zhang, L., Luo, J., Wan, P., Wu, J., Laski, F. and Chen, J.** (2011). Regulation of cofilin phosphorylation and asymmetry in collective cell migration during morphogenesis. *Development* **138**, 455-464.
- Zhou, W. and Hong, Y.** (2012). *Drosophila* Patj plays a supporting role in apical-basal polarity but is essential for viability. *Development* **139**, 2891-2896.

Figures

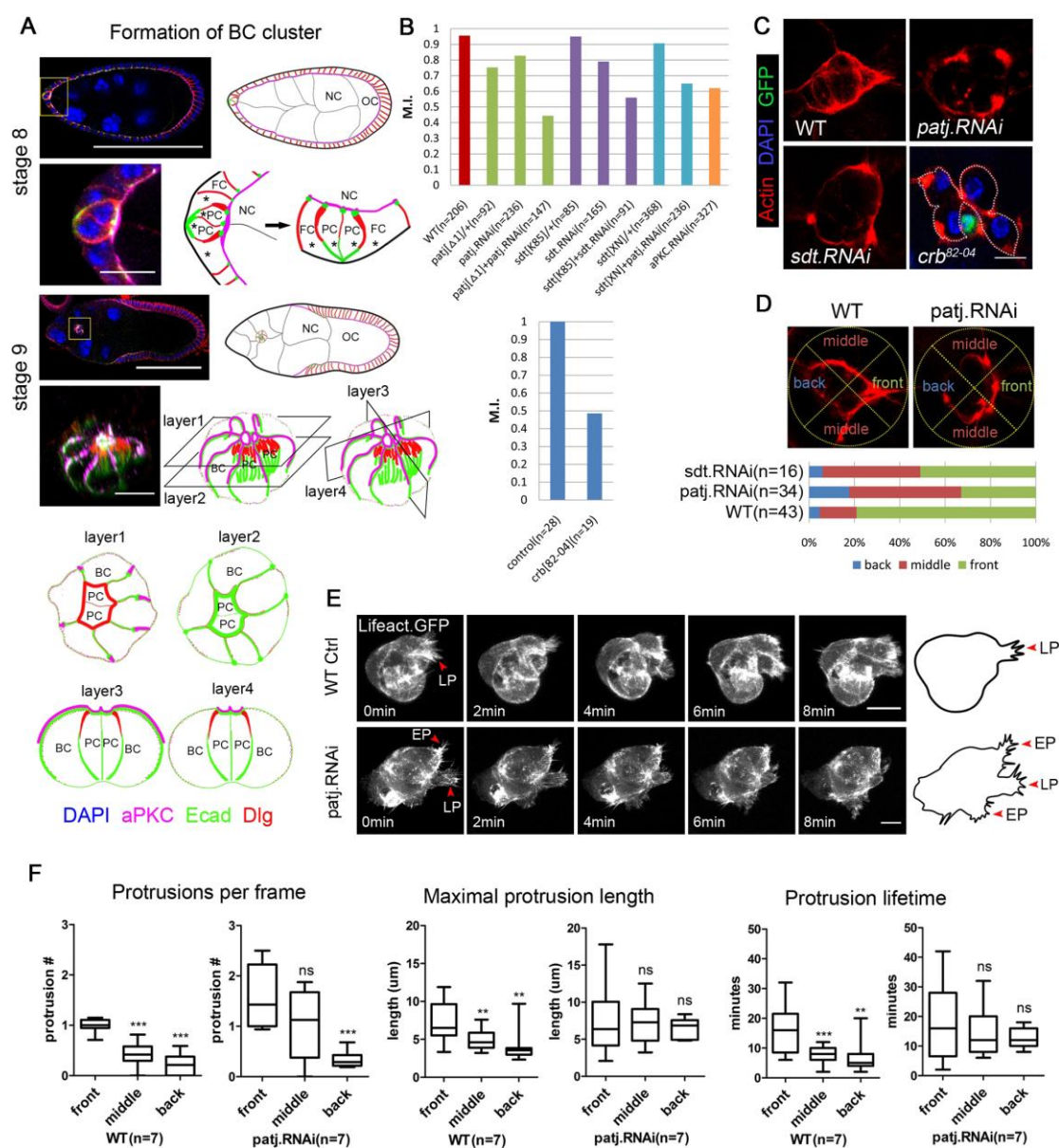


Fig. 1. Crb complex is required for border cell migration and front-back polarity.

(A) Diagrams showing distribution pattern of apical complex (stained with aPKC, violet), adherens junction complex (stained with E-cadherin, green), and the lateral complex (stained with Dlg, red) in the two anterior polar cells (PC) and surrounding follicle cells (FC), before and after formation of border cell cluster (stage 8 and stage 9 respectively). During migration, the border cell cluster detaches from the follicle epithelium, migrates between the large nurse cells (NC), and reaches the border

between NCs and oocyte (OC). The diagram of the migrating border cell cluster depicts a top view of the cluster. Layers 1-4 represent four cross-sectional views of the cluster, layer 3 is shown at a comparable view to that of the enlarged stage 8 precluster (top). (B) Migration index (MI) of border cells with different genotypes, see Materials and Methods for how MI is calculated. Also see Fig. S1A,B,D for detailed migration defects for these genotypes. (C) Wild type (WT) border cell cluster displayed a prominent actin-rich protrusion at the front, loss of function of *Crb*, *Sdt*, and *Patj* each resulted in ectopic actin patches at the side or back positions. (D) As the cluster is divided into three sectors (front, middle and back), the actin patches of *sdt RNAi* and *patj RNAi* were distributed throughout the three sectors, displaying a reduction of polarized distribution (as in WT) at the front. (E) Live cell imaging using Lifeact-GFP (labeling the F-actin) (Riedl et al., 2008) confirms that the ectopic actin patches are dynamic lamellipodial protrusions, see also Fig. S3 that confirms actin patches are protrusions. LP, leading protrusion; EP, ectopic protrusion. (F) The average number of sizable protrusions per frame (from 7 movies of border cell clusters for either WT or *patj RNAi*), maximal protrusion length, and duration (lifetime) of protrusion extension were measured, quantified and represented by the box and whisker plots. The box ranges from the 25th to the 75th percentiles, the whiskers represent the minimum and maximum values, and the line indicates the median value for this and all subsequent figures (Fig. 3-7). not significant (n.s.); ** $P < 0.01$; *** $P < 0.001$; unpaired t-test. Compared to WT, *patj RNAi* border cell clusters display different protrusion formation pattern (more side protrusions), longer protrusion length at all positions and longer duration during protrusion extension. (A-E) For all images of border cell clusters in this figure and all subsequent figures, anterior is to the left and posterior to the right, and the migration direction is to the right. In this and all subsequent figures, *Slbo-Gal4* driver is used for all genetic experiments (except for Flip-out experiments) involving expression of transgenes. For low magnification view of egg chambers (A), the scale bars are 100 μm , for all other images, scale bars: 10 μm .

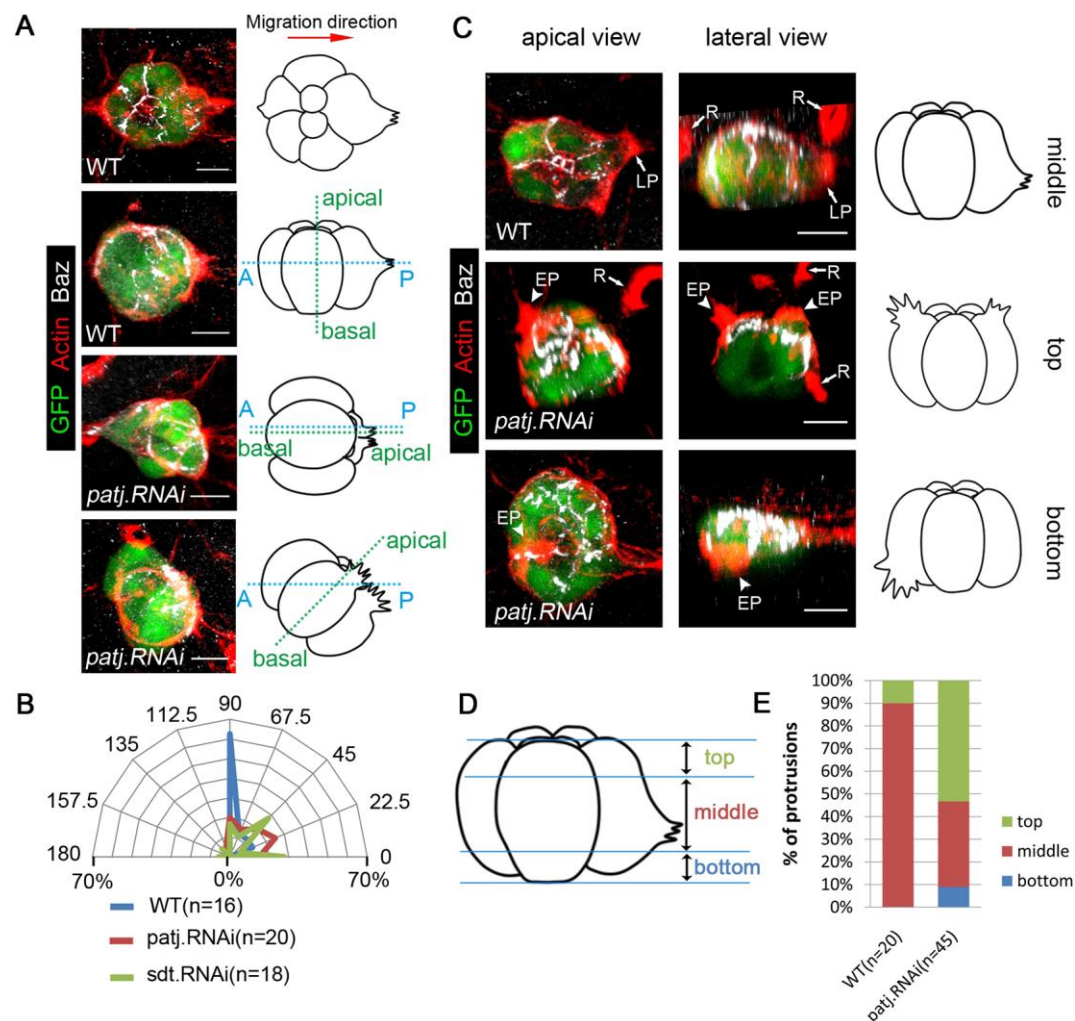


Fig. 2. Sdt and Patj are required for positioning of the apical-basal axis of border cells.

(A) During migration, the apical-basal axis of a wild type (WT) border cell cluster is almost always perpendicular to or at 90° angle to its migration direction, which is along the anterior-posterior (A-P) axis of the egg chamber. This is indicated by the two upper images of WT clusters at the apical view and lateral view respectively. For *patj* or *sdt* RNAi clusters, their apical-basal axes appeared at random angles to its migration direction, or A-P axis, as the lower two images of *patj* RNAi clusters indicate. Baz stained the apical junctions between adjacent border cells and between border cells and polar cells in both WT and *patj* RNAi clusters. GFP is a cytoplasmic marker of border cells. Each image in (A) and (C) was generated from a z-series of

confocal sections that were then subjected to 3D reconstruction (see Materials and Methods for details). (B) The radar map records the distribution of percentages of clusters with angles between apical-basal axis and A-P axis from 16 WT, 20 *patj RNAi* and 18 *sdt RNAi* border cell clusters. (C) Top panels: a WT cluster extending a prominent protrusion at the front from both apical and lateral views. The lateral view shows the leading protrusion extending from the lateral (or middle) region of the front border cell, as depicted in the diagram to the right. Middle and bottom panels: two *patj RNAi* clusters extending two ectopic protrusions at the apical (or top) region and one ectopic protrusion at the basal (or bottom) region respectively. (D, E) Quantification of distribution of protrusions from 20 WT clusters and 45 *patj RNAi* clusters. In WT, about 90% of protrusion formed in the middle region, which is defined as 50% (middle half) of the apical-basal axis. But protrusions from *patj RNAi* clusters lost their restricted positioning in the middle region, more than half of protrusions extended from the top region, which includes top 25% of the entire length of apical-basal axis. Scale bars: 10 μ m.

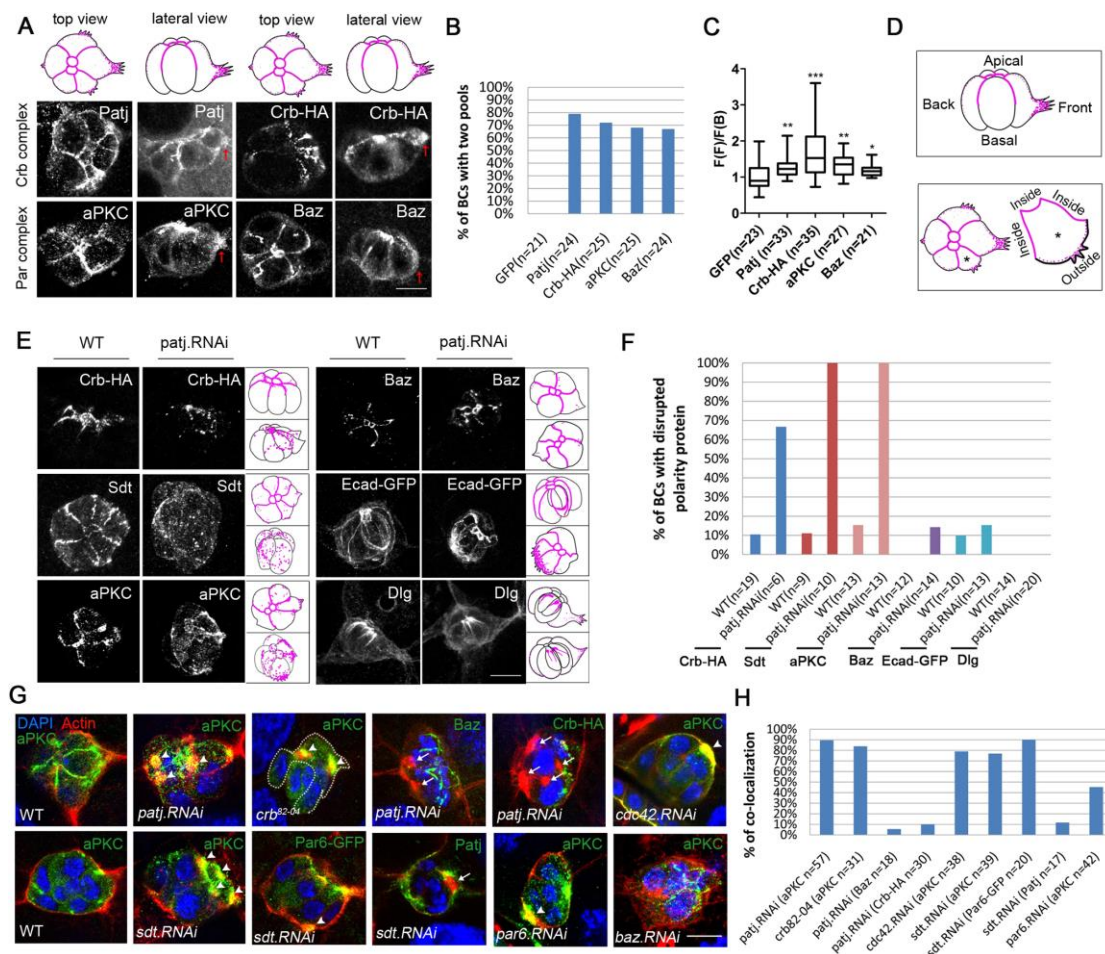


Fig. 3. Loss of Crb complex components causes disruption in distribution of apical polarity molecules and ectopic distribution of aPKC in actin patches.

(A-C) Confocal images showing the distribution of Crb complex components (Crb and Patj) and Par complex components (aPKC and Baz). Two distinct pools were present when viewed from top or laterally, the major pool at the apical junctions and the minor pool near the outside membrane. Red arrows point to the position of leading protrusions. Percentages of clusters showing distribution of two distinct pools are quantified in (B). Note some of the components including aPKC displayed polarized distribution toward the front of clusters (lateral view), front polarized distribution is quantified as F(Front)/F(Back), or Fluorescence intensity of the second pool at the front vs. at the back (C). * $P < 0.05$; ** $P < 0.01$; *** $P < 0.001$; unpaired t-test. See Materials and Methods for more details. All images are from single confocal sections.

(D) A schematic diagram depicting polarized distribution of apical molecules such as aPKC, as described in (A). Three distinct polarities are evident in the distribution pattern, including front-back polarity for the cluster, apical-basal polarity and inside-outside polarity for each border cell. (E, F) Confocal images (E) show that reduction of Patj severely disrupted the distribution of Crb-HA (from a knock-in allele of *crb*), Sdt and aPKC in the apical junctions, but did not grossly affect the junctional pattern of Baz, E-cad-GFP (a knock-in allele of *shg*) and the lateral polarity molecule Dlg. Results are quantified in (F). All images are based on maximum projection of z-stacks of confocal sections. Schematic representations of the images are to the right (top and bottom diagrams correspond to the left and right images respectively). (G,H) Loss of function of Crb complex components (Crb, Sdt and Patj) and Par complex components (Par6 and Cdc42) except for Baz resulted in severe disruption of the apical junction pool of most apical polarity components. But loss of Baz did not grossly affect the apical junctional pattern of aPKC. The images of patj RNAi (with Baz staining) and baz RNAi (with aPKC staining) are a result of maximum projection of z-stacks of confocal sections, all the other images are single confocal sections. The results are further quantified in (H) as percentages of clusters displaying strong colocalization of cytoplasmic aPKC or Par6-GFP spots with actin patches (colocalizations indicated by white arrowheads in G). Whereas white arrows indicate that cytoplasmic spots of other polarity components (Crb, Patj and Baz) do not colocalize with ectopic actin patches (G). Note that apical junctional aPKC do not normally colocalize with strong actin stainings in the apical and sub-apical plane (WT, top panel) or in the lateral plane (WT, bottom panel). Dashed line highlights *crb* mutant clone. Scale bars: 10 μ m.

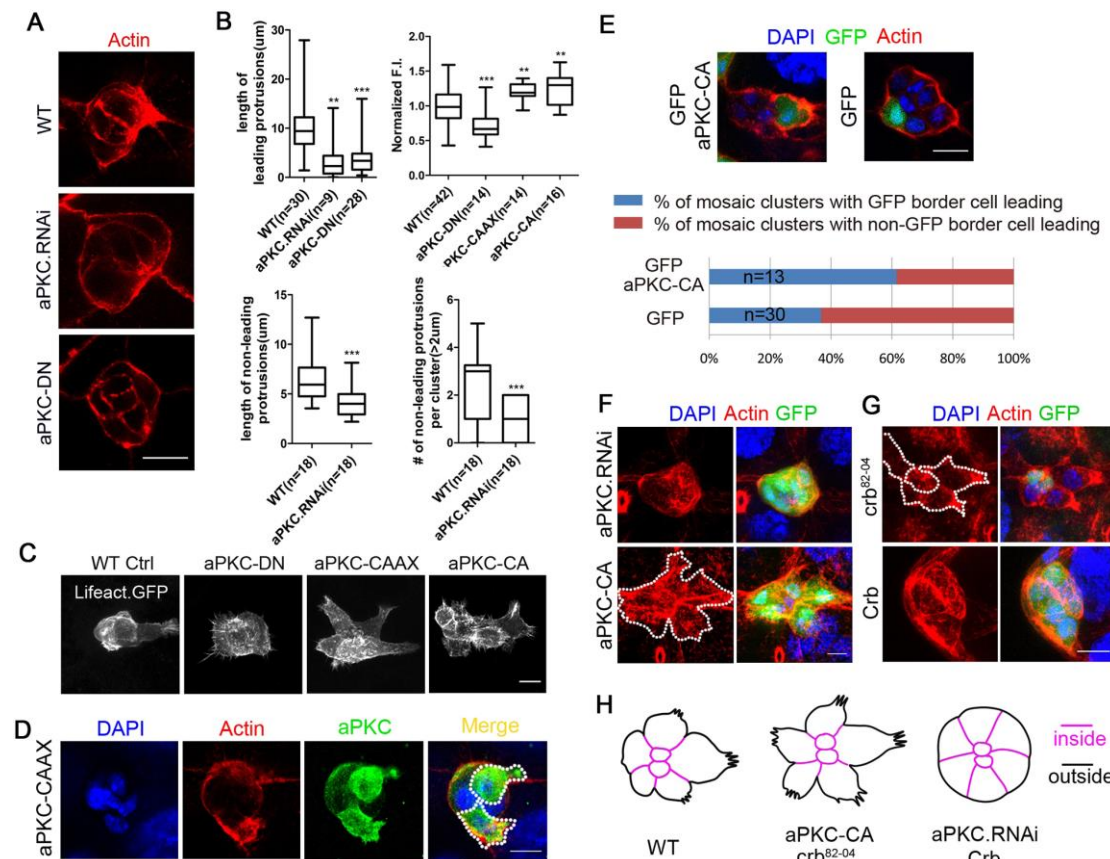


Fig. 4. aPKC is necessary and sufficient for formation of actin-enriched protrusions of border cells and may play roles in inside-outside polarity.

(A) Representative confocal images show that WT border cells display more protrusions, longer protrusions and increased levels of F-actin in protrusions and at their outside membranes than *aPKC RNAi* and *aPKC-DN* border cells. (B) Quantification of the above phenotypic differences in graphs, which demonstrate strong reduction in length of leading protrusions, length of non-leading protrusions, number of non-leading protrusions and normalized fluorescence intensity (F.I.) of F-actin staining in *aPKC RNAi* and *aPKC-DN* border cell clusters. Contrarily, F.I. of F-actin levels of *aPKC-CAAX* and *aPKC-CA* clusters were significantly increased. *, $P<0.05$; **, $P<0.01$; ***, $P<0.001$. (C) Representative images from time-lapse movies (see also Movie 5) showing WT control, *aPKC-DN*, *aPKC-CAAX* and *aPKC-CA* border cell clusters. *UAS-Lifeact-GFP* was driven by *slbo-Gal4* to express Lifeact-GFP, which labels F-actin *in vivo* (Riedl et al., 2008). Each image is a result of

maximum projection of a z-series of confocal sections (see Materials and Methods).

(D) Two individual border cells expressing aPKC-CAAX within an otherwise wild type cluster resulted in autonomous protrusion formation and enlargement. Dashed lines highlight two flip-out clones.

(E) Two Mosaic clusters that contain an aPKC and GFP expressing single-cell clone at the leading position (left) and a GFP expressing single-cell clone at non-leading position (right, control). *Ay-Gal4/UAS-GFP*, *UAS-transgene* generates a flip-out clone co-expressing GFP and the desired transgene within a wild-type cluster. Mosaic clusters were scored for the percentages of clusters showing the GFP expressing cell leading or non-GFP cell leading, demonstrating that local and autonomous increase of aPKC activity in the single cell biased it to become the leading cell.

(F, G) Border cells with aPKC-CA expression or with *crb*⁸²⁻⁰⁴ mutation displayed an outstretched phenotype (cluster outlined by dashed line), which indicate that increased proportion of border cell membrane became outside (more dynamic) membrane. Border cells with aPKC RNAi expression or Crb overexpression displayed a more compacted cluster with less protrusion and membrane dynamics than WT, an opposite phenotype from that of *crb*⁸²⁻⁰⁴ mutant or aPKC-CA expressing clusters. All images in (F, G) are a result of maximum projection of z-stacks of confocal sections, and they are represented schematically in (H). Scale bars: 10 μ m.

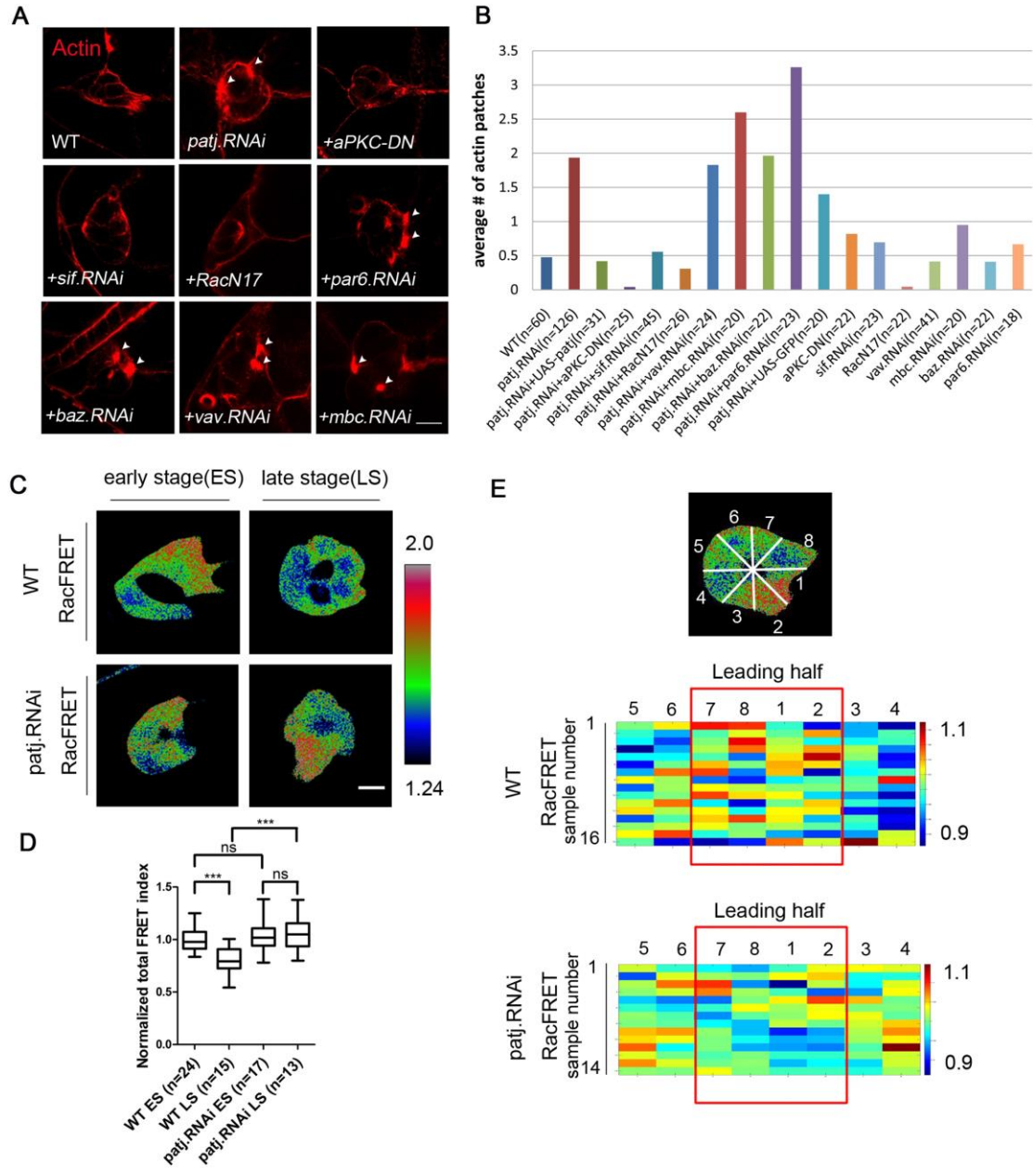


Fig. 5. aPKC, Sif and Rac mediate the formation of ectopic protrusions as resulted from loss of Patj.

(A) Loss of Patj resulted in ectopic actin patches or protrusions, which could be rescued by loss of function of aPKC, Sif, Rac but not by downregulation of Par6, Baz, Vav and Mbc. (B) Quantification of ectopic actin patches by *patj RNAi* and their rescue by various transgenes. (C) Representative Rac-FRET patterns in WT control and *patj RNAi* border cells, both during early stage and late stage of migration. Note that Rac-FRET reporter was not expressed in the polar cells and thus the FRET signal was excluded from the central area of clusters. (D) Total FRET indices of late stage (LS) WT and *patj RNAi* border cell clusters, as normalized against that of early stage (ES) WT clusters. Note there is no difference in Rac-FRET index between early stage and late stage *patj RNAi* clusters, so staging was not applied to *patj RNAi* clusters in other figures. (E) Distribution of Rac-FRET signals from 16 control samples and 14 *patj RNAi* samples at early stage were plotted in the heat maps. Numbers on the X-axis correspond to 8 divided sectors as shown in the top image. Each row represents FRET signal distribution of one sample cluster, where 7, 8, 1, 2 indicate the leading half of the cluster. Scale bars: 10 μ m.

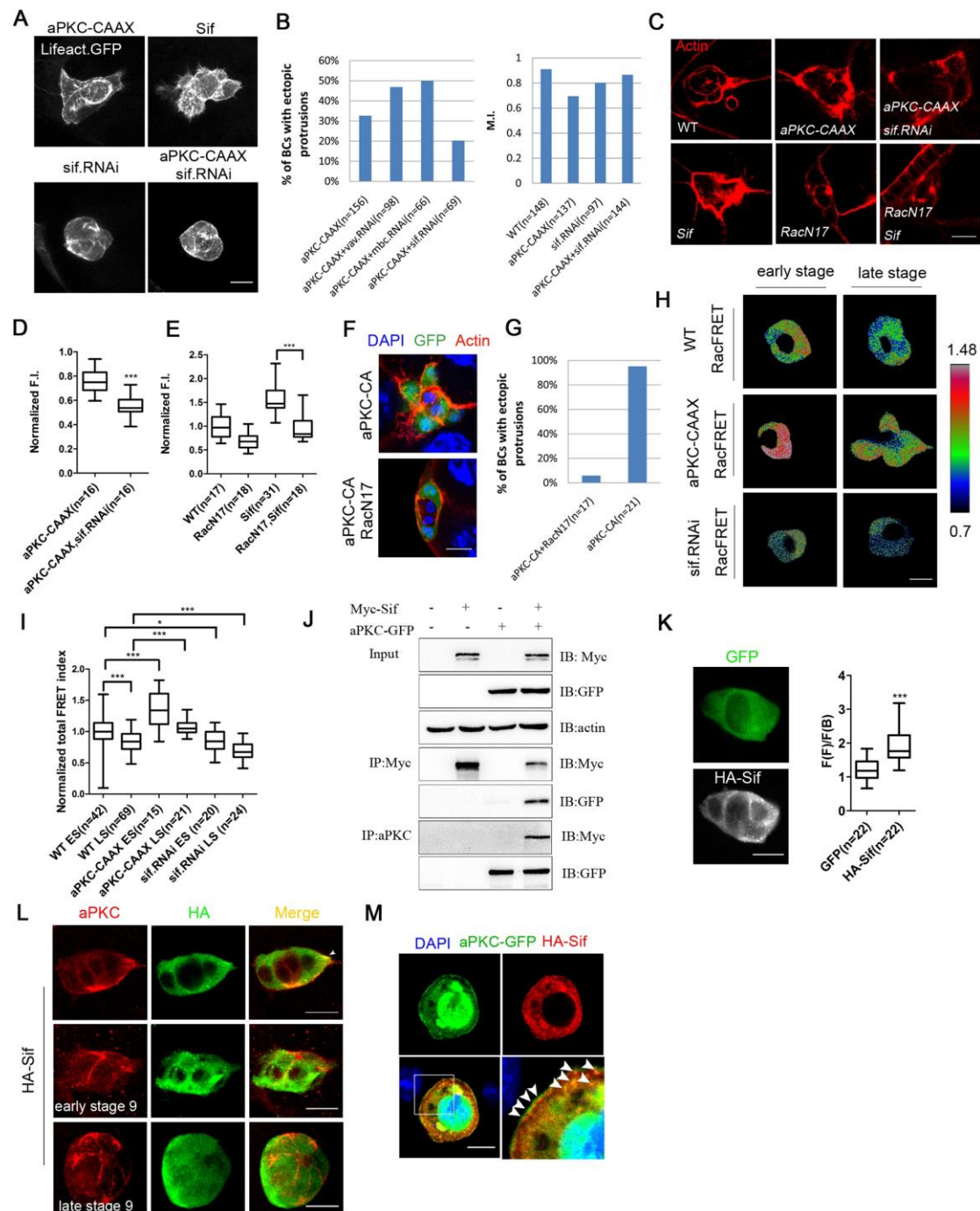


Fig. 6. aPKC acts upstream of Sif and Rac to promote actin-based protrusions.

(A) As the time lapse images indicate, aPKC-CAAX overexpression caused increased levels of F-actin (labeled by Lifeact-GFP) and large ectopic protrusions, which are similar to those caused by Sif overexpression and could be rescued by *sif RNAi*. (B) The left graph shows that *sif RNAi* but not *vav* or *mbc RNAi* could rescue the ectopic protrusion as resulted from aPKC-CAAX overexpression. The right graph displays

that the reduced migration index (MI) of aPKC-CAAX expressing clusters was mostly restored by coexpression of *sif RNAi*, which alone caused moderate reduction of MI. (C-E) Increase of F-actin levels by aPKC-CAAX expression was rescued by *sif RNAi* coexpression, and increase of F-actin levels by Sif expression was rescued by RacN17 co-expression. (F, G) The strong ectopic protrusion phenotype of aPKC-CA border cells could be rescued by expression of the dominant negative RacN17. (H) Representative Rac-FRET patterns in WT control, aPKC-CAAX and *sif RNAi* border cells, during early stage and late stage of migration. (I) Total FRET indices of late stage (LS) WT and other transgene-expressing border cell clusters, as normalized against that of early stage (ES) WT clusters. (J) From the immunoprecipitation (IP) of Myc-Sif from lysate of *Drosophila* S2 cell transfected with both Myc-Sif and aPKC-GFP, aPKC-GFP was found in significant level as indicated by immunoblot (IB). From reciprocal IP of aPKC-GFP, Myc-Sif was also found in significant level. (K) A representative image of HA-Sif and GFP co-expressing border cells, with uniform GFP (as a control) distribution and front-polarized HA-Sif distribution, as quantified in the graph below. The confocal sections are taken at the lateral position along apical-basal axis, where protrusion is clearly visible. (L) Staining of Sif expressing border cell clusters with aPKC and HA-Sif. Top panels represent a single confocal section at the lateral position, where protrusions are visible and aPKC and HA-Sif are shown to significant overlap near protrusions and membrane (marked by arrowhead). The middle and bottom panels represent stacks of confocal z-series that are subjected to maximum projection. The region stained by aPKC is the apical junction and most of Sif-HA occupies the basal-lateral region of border cells at early or late stage 9. (M) Confocal images showing a *Drosophila* S2 cell co-transfected with aPKC-GFP (green) and HA-Sif (red). aPKC-GFP was partially colocalized with HA-Sif (yellow) at cell cortex and cytoplasm. The bottom right panel is a high-magnification view of the square region marked in the image to the left. Arrowheads point to colocalized dots. Scale bar for (M): 5 μ m; for all other panels: 10 μ m.

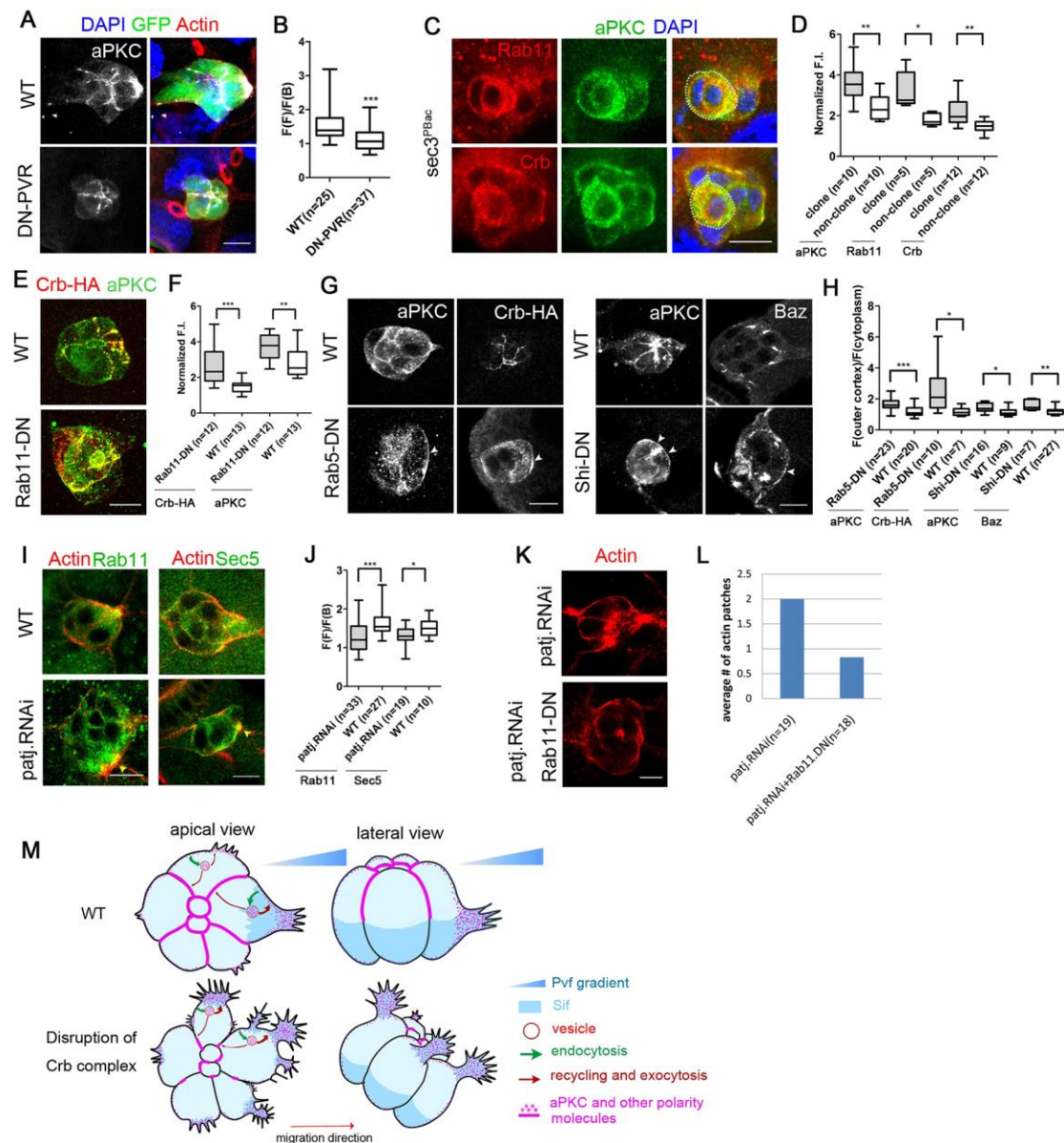


Fig. 7. Endocytic recycling mediates formation of ectopic protrusions and regulates the polarized distribution of two distinct pools of aPKC.

(A, B) The front polarized localization of aPKC near the lateral outside membrane in WT border cells was absent in DN-PVR expressing border cells. Front-back ratios were quantified in (B). Each image was generated as a maximum projection of a z-stack of confocal sections. (C, D) Disruption of normal distribution patterns of aPKC and Crb in mosaic clusters containing homozygous *sec3*^{PBac} clones (encircled by dotted white lines), which is quantified in a graph of levels (as normalized

Fluorescence intensity (FI)) of cytoplasmic polarity proteins and Rab11 in mutant clone and in non-mutant cells. (E-H) Disruption of distribution patterns of aPKC, Crb-HA and Baz by expressing dominant negative forms of Rab11 (Rab11-DN), Rab5 (Rab5-DN) and Shi (Shi-DN) in all border cells. Crb-HA was endogenously expressed from a knock-in locus of *crb*. Phenotypes were quantified as increased levels of aPKC or Crb-HA staining in the cytoplasm in (E, F), and as ratios of polarity protein levels on the outside membrane over their levels in the cytoplasm (G, H). (I, J) Distribution pattern of Rab11 and Sec5 in WT and *patj RNAi* border cells. Strong staining of Rab11 or Sec5 was shown to be adjacent to and overlapping with an ectopic actin patch (labeled by yellow arrowhead). Front-polarized distributions were quantified as front-back ratios in (J). (K, L) The dominant negative form of Rab11 (Rab11DN) suppressed the ectopic actin patch phenotype by *patj RNAi*. (M) Schematic diagram of the proposed model. Mechanism details are explained in Discussion. Scale bars: 10 μm .

Supplementary Figures

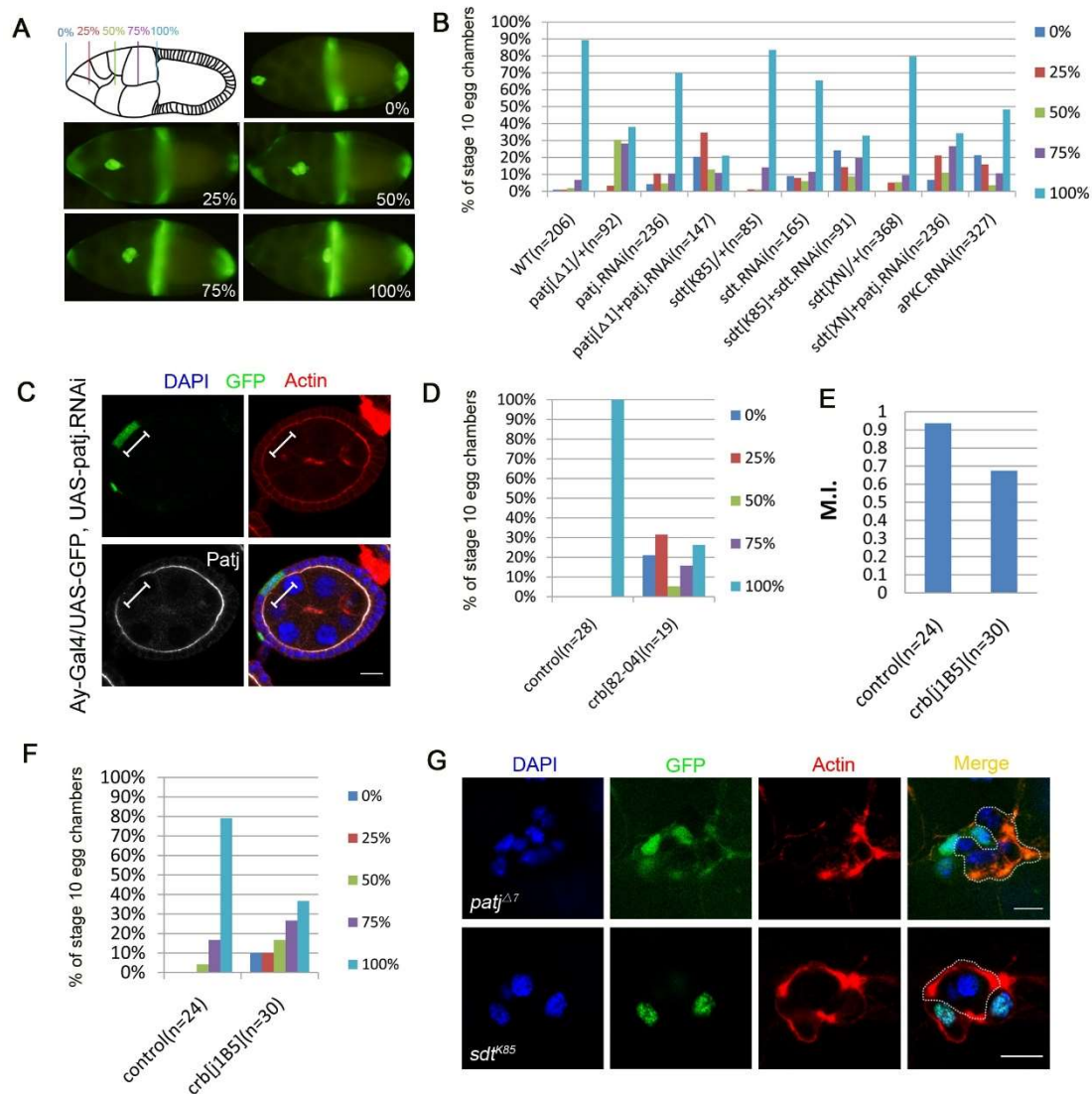


Figure S1. Crb complex components and aPKC are required for border cell migration.

(A) A diagram and fluorescent images showing the extent of border cell migration for stage 10 egg chambers. In wild type, border cells normally have completed posterior migration at stage 10, and it is represented in the “100%” migration category. The categories of 0% (no migration), 25%, 50% and 75% represent different degrees of migration delay. (B, D-F) Quantification of border cell migration. The Y-axis denotes the percentage of stage 10 egg chambers that exhibit each degree of migration, as represented by five color-coded bars for each genotype (B, D, F). (E) Migration index

(MI) of mosaic border cell clusters containing *crb*^{1B5} mutant clones, the detailed migration delay analysis is in (F). (C) An egg chamber contains a Flip-out follicle cell clone that expressed *patj RNAi*. Antibody staining revealed that Patj level was strongly reduced in the clone. (G) Mosaic border cell clusters containing *patj* or *sdt* mutant clones resulted in ectopic actin patches. Dashed lines outline the *patj* or *sdt* mutant clone. Scale bars: 10µm.

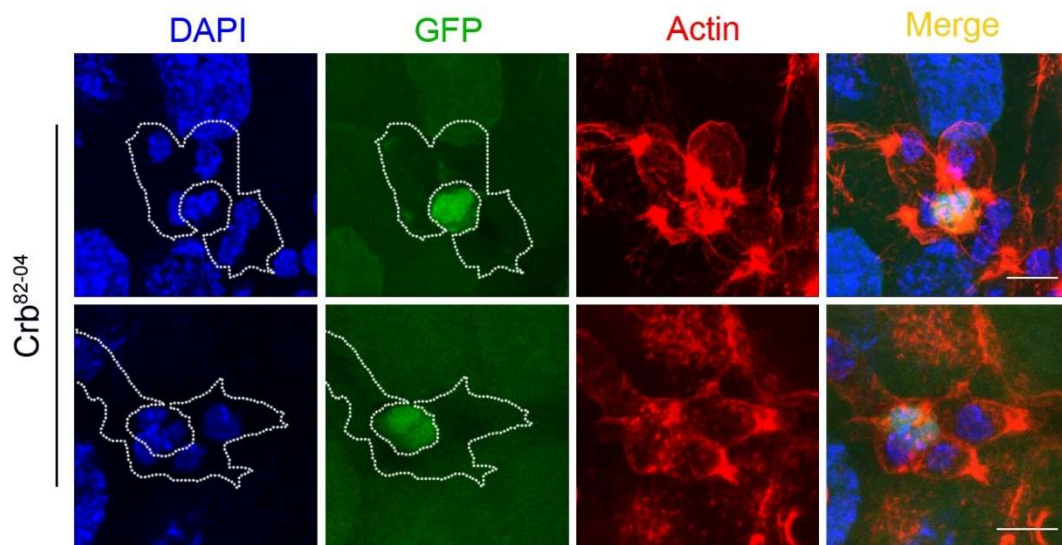


Figure S2. The *crb*⁸²⁻⁰⁴ phenotype of ectopic actin patches is autonomous to border cells. The top row and bottom row each shows a mosaic cluster containing two central polar cells that are wild type or heterozygous (GFP positive, their DAPI-labeled nuclei smaller than those of adjacent border cells). The rest of the mosaic cluster is composed of a clone of *crb*⁸²⁻⁰⁴ mutant outer border cells, which are indicated by lack of GFP and outlined by a dashed line. Wild type polar cells do not prevent the entire cluster from exhibiting the ectopic actin patches phenotype. The *crb*⁸²⁻⁰⁴ mosaic cluster shown in the top row is the same cluster shown in Fig. 1C, except that the images here are derived from maximum projection of a z-series of confocal sections but the image in Fig. 1C is

a single confocal section. The bottom mosaic cluster is also shown in Fig. 4G, and the images are all resulted from maximum projection of a z-series of confocal sections.

Scale bars: 10 μ m.

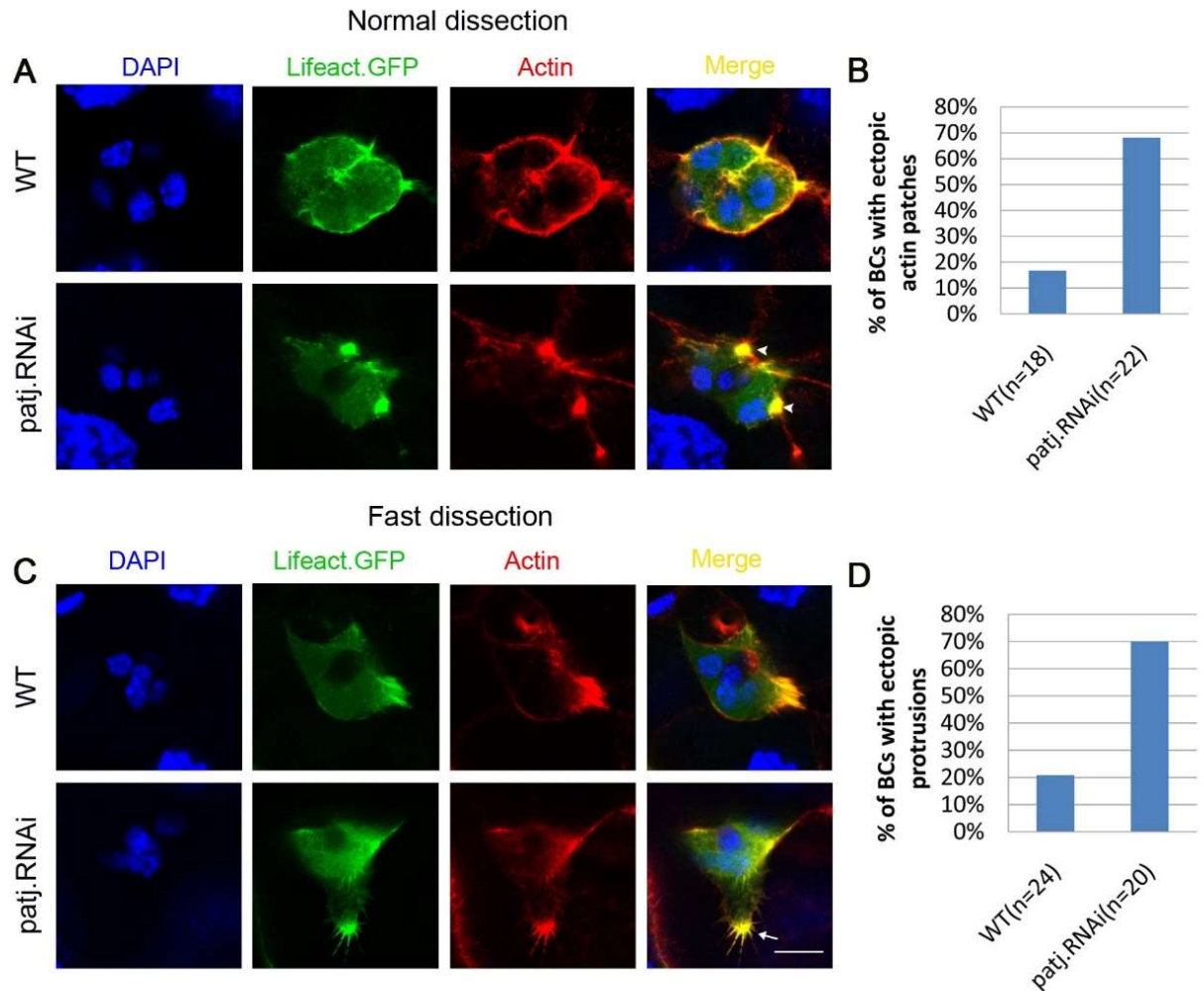


Figure S3. Fast dissection reveals fine structures of ectopic actin patches.

(A, B) After normal dissection and immunostaining (ovaries were dissected in cold PBS and the process would last about 20 minutes or above), typical wild type (WT) border cells extended a leading protrusion at the front, but *patj RNAi* border cells exhibited large ectopic actin patches at the side of cluster. Arrowheads indicate actin patches. Quantification for actin patches indicates that 68% of *patj RNAi* expressing border cell clusters (n=22) displayed ectopic actin patches. (C, D) After fast dissection and staining

(ovaries were dissected in cold PBS but the whole process was limited to less than 5 minutes), both the predominant protrusion at the leading edge in WT border cells and the ectopic actin patch in *patj* RNAi border cells exhibited finer details, which are characteristics of lamellipodial protrusion. Arrow indicates ectopic protrusion. Quantification indicates that 70% of *patj* RNAi clusters (n=20) displayed ectopic protrusions with fast method. The above results nicely confirmed that the actin patches observed using normal method are actually ectopic protrusions that displayed dynamic actin structures. F-actin is labeled by both Lifeact-GFP (green) and phalloidin-TRITC (red). Scale bar: 10 μ m.

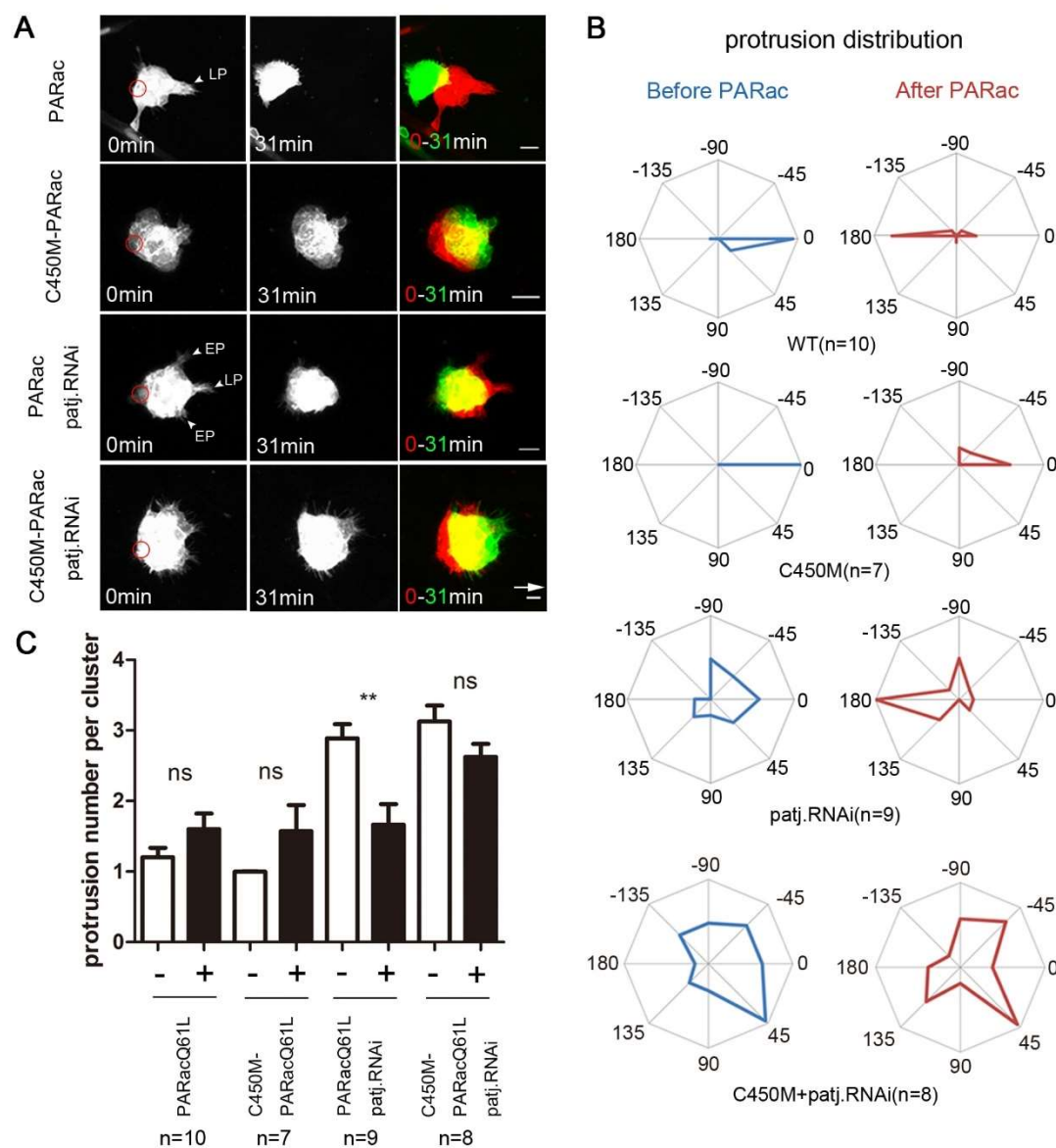


Figure S4. Loss of Patj does not affect non-autonomous cell-cell communication.

(A) Confocal images in the top panels (WT control) show that local photoactivation of PA-Rac by laser (red circle) in the back border cell induced a new protrusion, caused retraction of the leading protrusion, and redirected the whole cluster to move in an opposite direction, demonstrating effective cell-cell communication between the back cell and leading cell. The second row panels show that photoactivation of the photo-insensitive C450M-PA-Rac failed to achieve the above results, serving as a negative control (Wang et al., 2010). The third row panels show that local photoactivation of PA-Rac in the back cell of *patj RNAi* cluster not only retracted the leading protrusion but also retracted two ectopic protrusions on the side. Redirection of collective movement of cluster was also achieved. On the contrary, the bottom panels show that photoactivation of C450M-PA-Rac in *patj RNAi* background failed to result in retraction of ectopic protrusions and redirection of migration. White arrow indicates border cells' normal migration direction, which is to the right for all figures. White arrowheads point to leading protrusion (LP) and ectopic protrusion (EP). (B) Analysis of protrusion distribution by radar diagram, which divides the border cell cluster into 8 sectors. In the WT control, most of protrusions were aligned toward 0° (front) before PA-Rac photoactivation, but were switched toward 180° (back) after photoactivation. Such a switch in protrusion distribution is evident in *patj RNAi* but not in the C450M negative controls. (C) Quantification of average protrusion number per cluster reveals that a strong and significant reduction of protrusion number between before photoactivation (-) and after photoactivation (+) was only observed for *patj RNAi*. **, $P < 0.01$; ns, not significant; unpaired t-test; error bars indicate s.e.m. Scale bars: 10 μm .

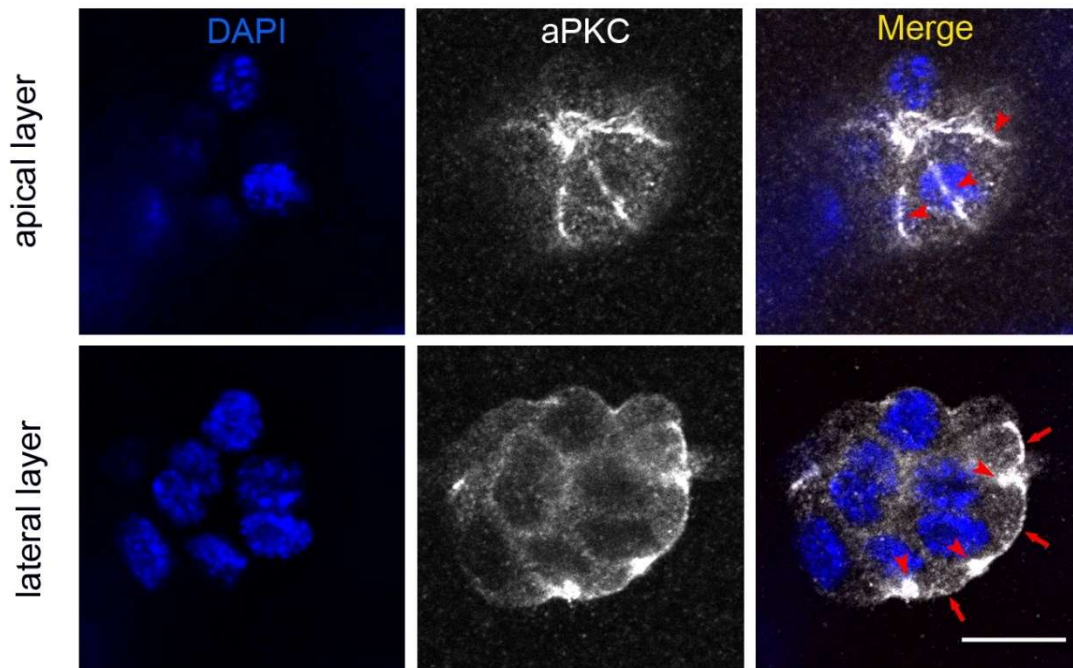


Figure S5. The two distinct pools of aPKC are best captured at two different focal planes within the same border cell cluster. The top row shows the single section confocal images of a border cell cluster at the apical layer/plane. Long lines of strong aPKC staining (indicated by red arrowheads) represent the major pool of membrane-bound aPKC at apical junctions between adjacent border cells. At this focal plane, the second minor pool of aPKC that is localized close to the outside lateral membrane is not obvious. Moving more basally to the lateral focal plane, the second pool of aPKC comes into view as thin lines or dots of moderate staining near the outside lateral membrane (indicated by red arrows) in the bottom row of confocal images. Meanwhile, the apical junctional staining of aPKC are mostly out of focus except for the remaining large spots (indicated by the red arrowheads), which are the most distal part of apical junctions between adjacent border cells. Note that between the large spots of junctional aPKC staining lies the second pool of aPKC (indicated by red arrows). Scale bars: 10 μm .

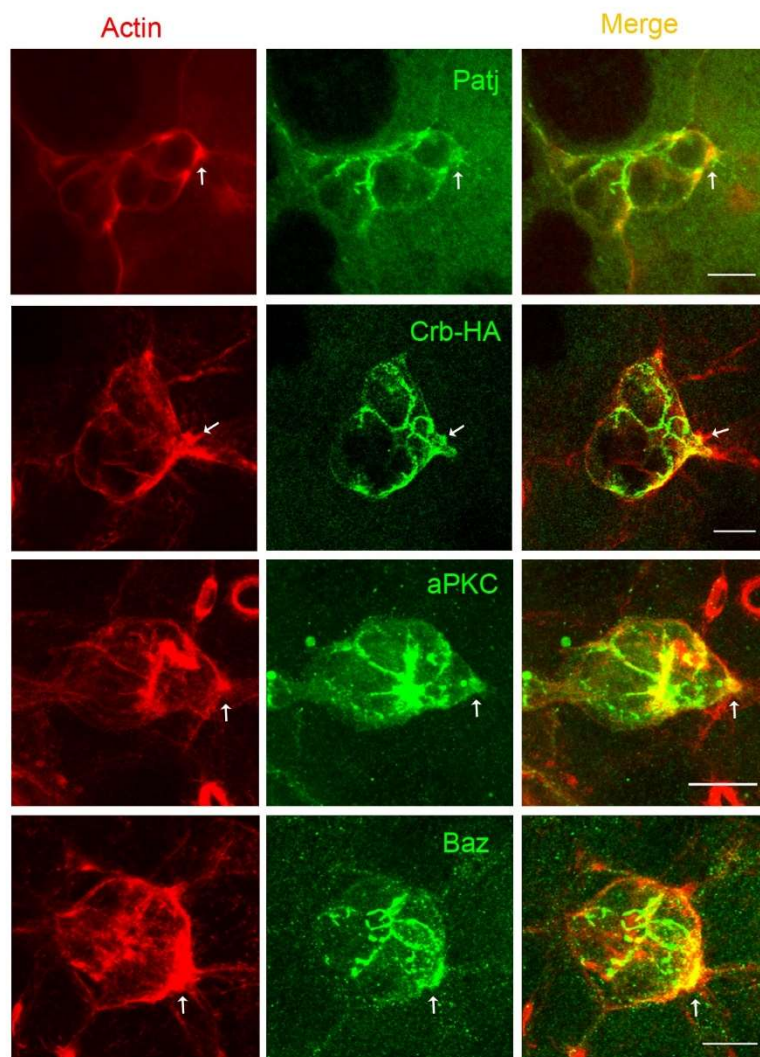


Figure S6. The second pool of apical polarity proteins is often observed to be enriched in leading protrusions. Patj, Crb-HA, aPKC and Baz are shown to be enriched (indicated by white arrows) in the leading protrusions of wild type border cell clusters. Because the apical junctional pool and the second pool near outside lateral membrane cannot be easily captured in one confocal image, we have to generate maximum projections of z-series to show both pools for Crb-HA, aPKC and Baz. The top row of Patj images is from single confocal sections, the same cluster is also shown in Fig. 3A (Patj). F-actin was labeled by phalloidin (red). Scale bars: 10 μ m.

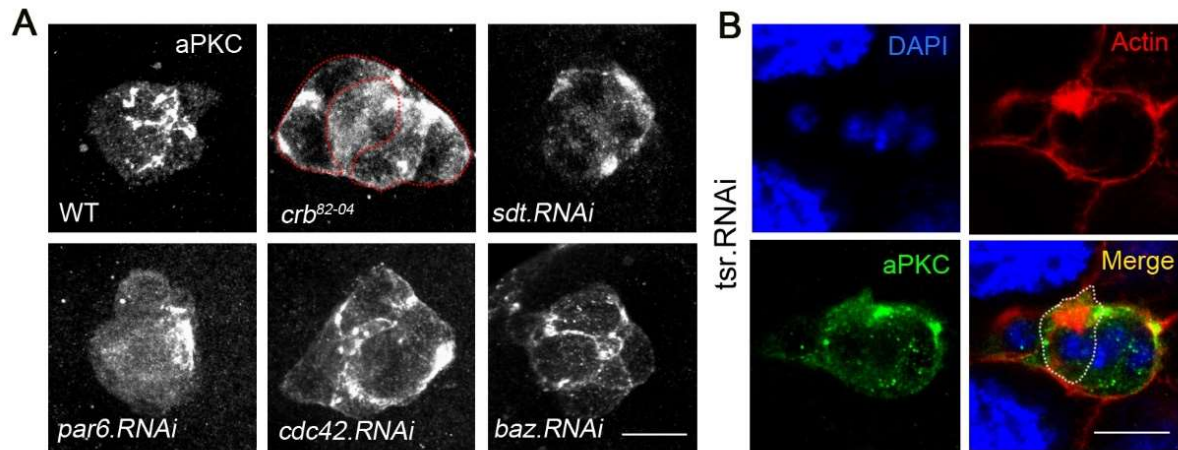


Figure S7. Distribution of aPKC caused by loss of function of Crb, Sdt, Par6, Cdc42, Baz and cofilin.

(A) Confocal images showing that loss of Crb complex components (Crb and Sdt) or Par complex components (Par6, Cdc42 but not Baz) severely disrupted the distribution of aPKC in the apical junctions. Reduction of Baz did not grossly affect the aPKC's distribution pattern. Dotted red line outlines the mutant *crb*⁸²⁻⁰⁴ clone in the cluster. (B) One border cell cluster containing a single cell flip-out clone expressing *tsr RNAi* (*tsr* encodes cofilin) resulted in a large ectopic actin patch inside the clone, but no aPKC staining was colocalized with the actin patch. Scale bars: 10µm.

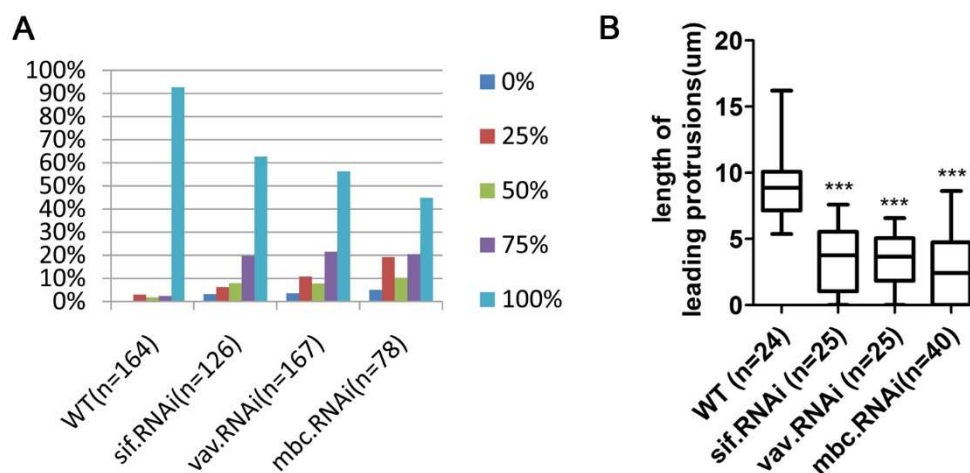


Figure S8. Knockdown of *sif*, *vav* or *mbc* resulted in migration defects and shortening of leading protrusions.

(A) *sif*, *vav*, or *mbc* RNAi each caused migration delay and (B) significant reduction of leading protrusion length, which is quantified and represented by the box and whisker plots. The box ranges from the 25th to the 75th percentiles, the whiskers represent the minimum and maximum values, and the line indicates the median value. *** $P < 0.001$; unpaired t-test.

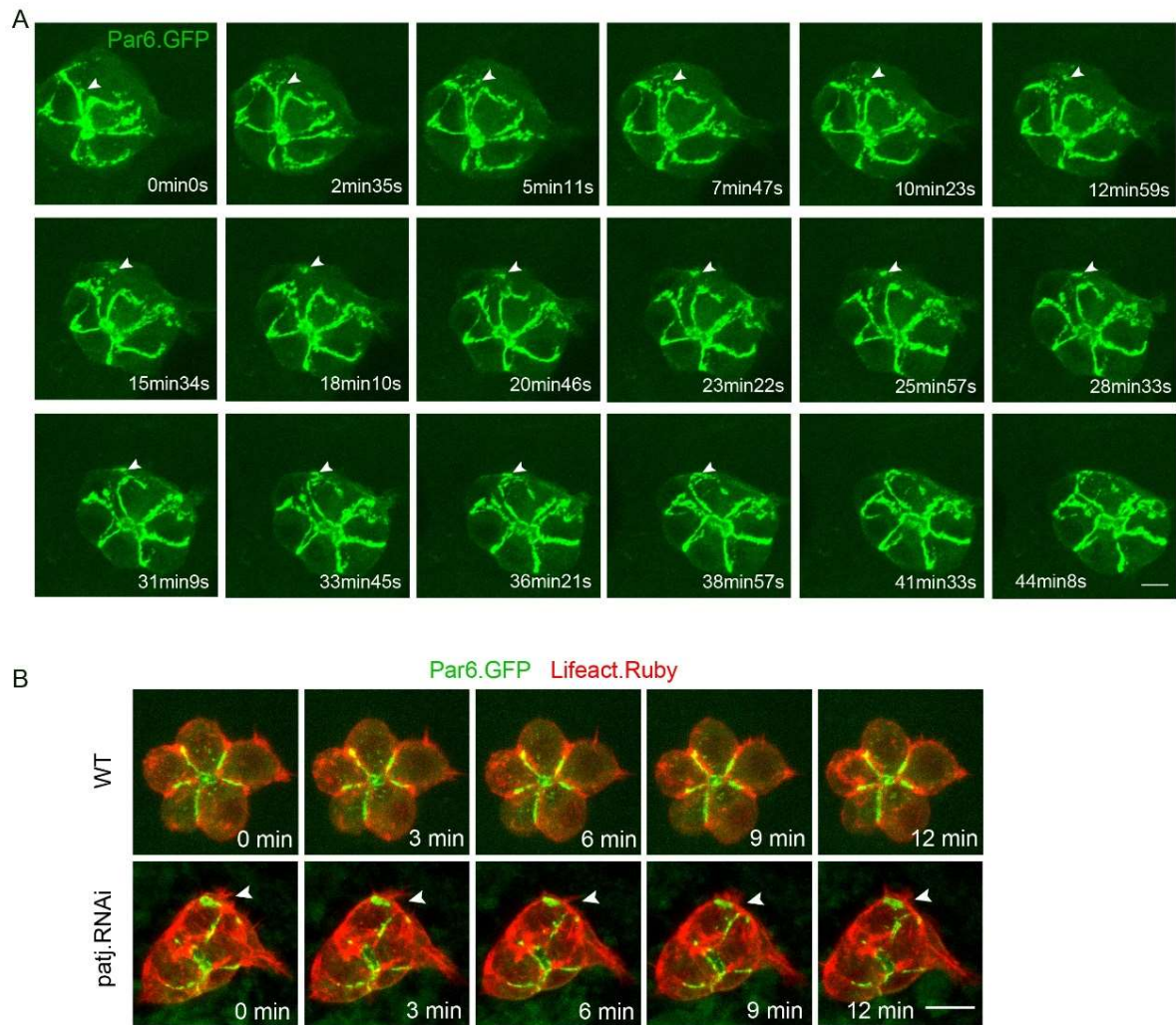


Figure S9. Dynamic distribution of Par6-GFP in WT and *patj* RNAi border cells.

(A) Time lapse images showing the dynamic distribution pattern of Par6-GFP in WT border cells. Par6-GFP signals mainly accumulated as lines at the apical junctions but they could be observed detaching from junctions as dots and moving toward the outer cortex. Arrowhead points to such a dot. (B) Time lapse images showing ectopic actin-rich protrusions extended from the position where an ectopic Par6-GFP patch was present as a result of loss of Patj (the second row), but this phenomenon could not be found in WT control (the first row). F-actin was labeled by Lifeact-Ruby (red). Arrowhead highlights the ectopic protrusion. Scale bar: 10µm.

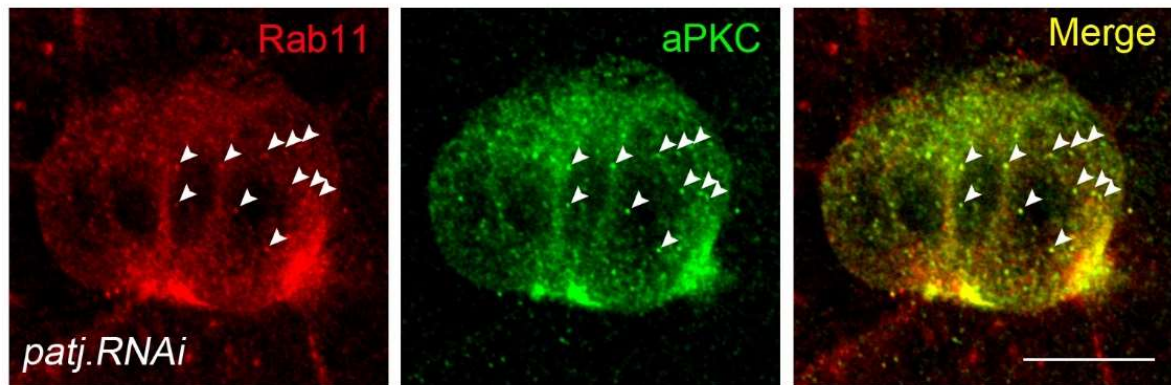
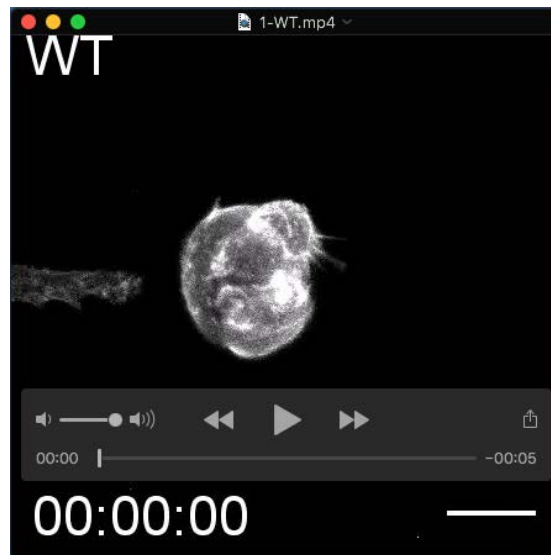


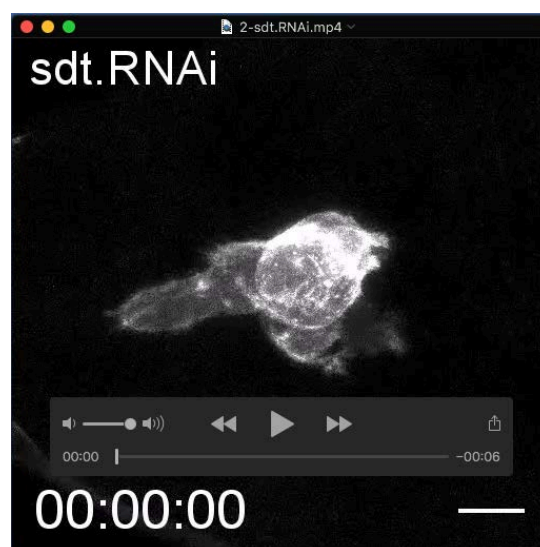
Figure S10. A high level of recycling is associated with large ectopic aPKC spots.

In *patj RNAi* border cells, locally enriched recycling vesicles/endosomes were shown to partially localize with large ectopic aPKC patches near the outside membrane. In addition, Rab11-labeled recycling vesicles were shown to clearly colocalize with small aPKC dots in the cytoplasm (colocalizations indicated by white arrowheads). The images were captured using the latest Zeiss 880 Airyscan technology for high resolution imaging (achieving a maximum resolution of 120 nm in the x-y plane according to the manufacturer, which is close to super resolution quality). Scale bar: 10 μ m.

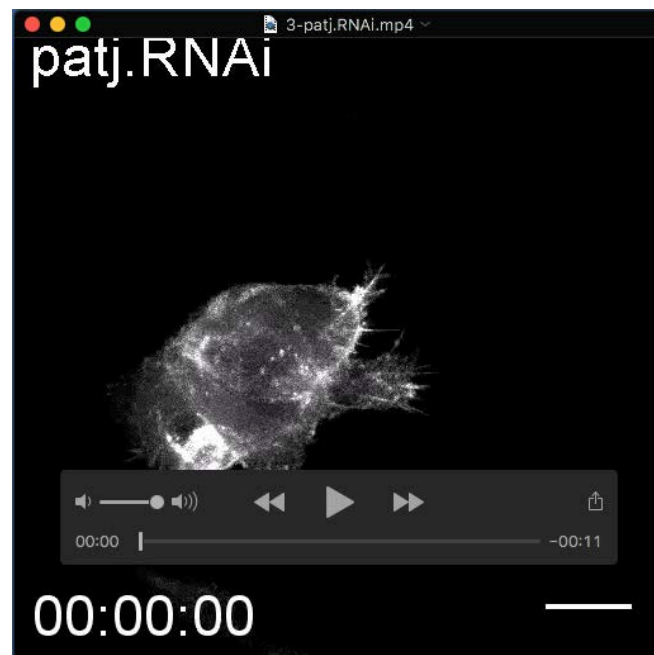
Movies



Movie 1. Live imaging of collective migration of a wild type (WT) border cell cluster. The border cells are shown migrating as a coherent cluster, with a large, predominant protrusion at the leading position. UAS-lifeact-GFP was expressed to label F-actin enriched structures such as protrusions in this and all subsequent movies. See Materials and Methods for details on live imaging. Scale bar: 10 μ m.



Movie 2. Live imaging of migrating border cells that are expressing *sdt RNAi*. The border cell cluster is shown extending several large ectopic protrusions during migration. The genotype of border cells is *slbo-Gal4*, *UAS-sdt RNAi*, *UAS-Lifeact-GFP*. All the transgenes and *RNAi* constructs were expressed using *slbo-Gal4*, a border cell-specific *Gal4* driver in this and subsequent movies. Scale bar: 10 μ m.



Movie 3. Live imaging of collective migration of *patj RNAi* expressing border cells. The *patj RNAi* border cells extend several ectopic protrusions in random directions during migration. Scale bar: 10 μ m.



Movie 4. Additional expression of *aPKC-DN* or *sif RNAi* rescues the ectopic protrusions phenotype exhibited by *patj RNAi* expression. Reducing the function of aPKC (by *aPKC-DN* expression), or Sif (by *sif RNAi* expression), in the background of *patj RNAi* expression, rescued the phenotype of ectopic protrusions. Note that the leading protrusions are also significantly shortened. Scale bars: 10 μ m.



Movie 5. Live imaging of border cell clusters expressing different mutant forms of aPKC. Expressing the dominant negative form of aPKC (aPKC-DN) resulted in suppression of leading protrusion formation, even though dynamic filopodial structures were seen forming randomly. In contrast, expression of the overactivated forms of aPKC (aPKC-CAAX and aPKC-CA) resulted in formation of large ectopic protrusions. Their clusters are much less coherent than the wild type clusters, individual border cells appear stretched outward. Scale bars: 10 μ m.



Movie 6. Sif overexpression resembles the aPKC-CAAX phenotype while *sif RNAi* rescues aPKC-CAAX's phenotype. Sif overexpression resembles the aPKC-CAAX phenotype that displays large ectopic protrusions and outstretched border cells. Expression of *sif RNAi* rescues aPKC-CAAX's phenotype. Scale bars: 10 μ m.



Movie 7. Expression of aPKC-DN fails to rescue the ectopic protrusions phenotype of Sif overexpression. Co-expression of the dominant negative form of aPKC (aPKC-DN) with Sif resulted in the same phenotype of expressing Sif alone. Scale bars: 10 μ m.

Supplementary Figures

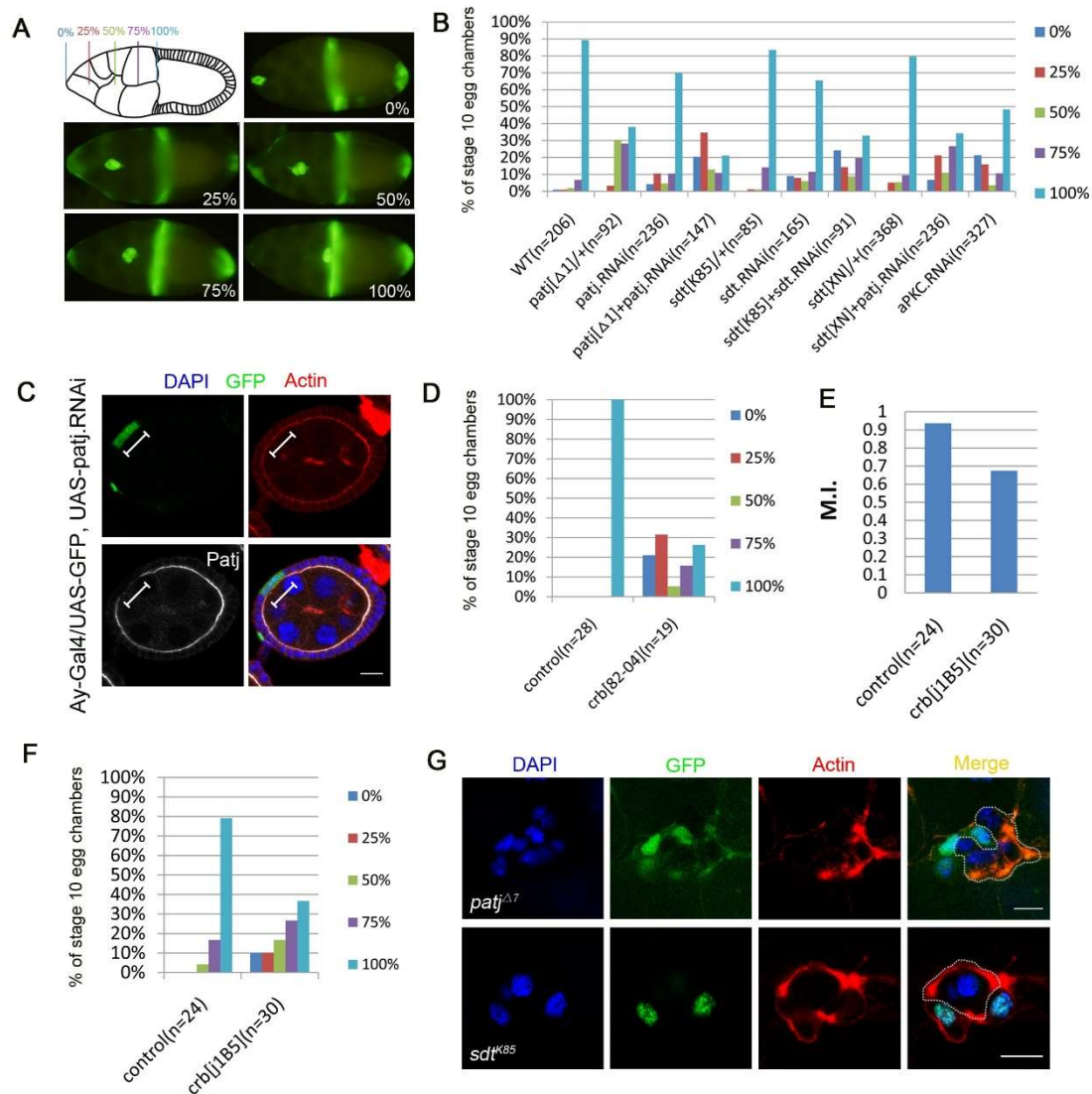


Figure S1. Crb complex components and aPKC are required for border cell migration.

(A) A diagram and fluorescent images showing the extent of border cell migration for stage 10 egg chambers. In wild type, border cells normally have completed posterior migration at stage 10, and it is represented in the “100%” migration category. The categories of 0% (no migration), 25%, 50% and 75% represent different degrees of migration delay. (B, D-F) Quantification of border cell migration. The Y-axis denotes the percentage of stage 10 egg chambers that exhibit each degree of migration, as represented by five color-coded bars for each genotype (B, D, F). (E) Migration index

(MI) of mosaic border cell clusters containing *crb*^{1B5} mutant clones, the detailed migration delay analysis is in (F). (C) An egg chamber contains a Flip-out follicle cell clone that expressed *patj RNAi*. Antibody staining revealed that Patj level was strongly reduced in the clone. (G) Mosaic border cell clusters containing *patj* or *sdt* mutant clones resulted in ectopic actin patches. Dashed lines outline the *patj* or *sdt* mutant clone. Scale bars: 10µm.

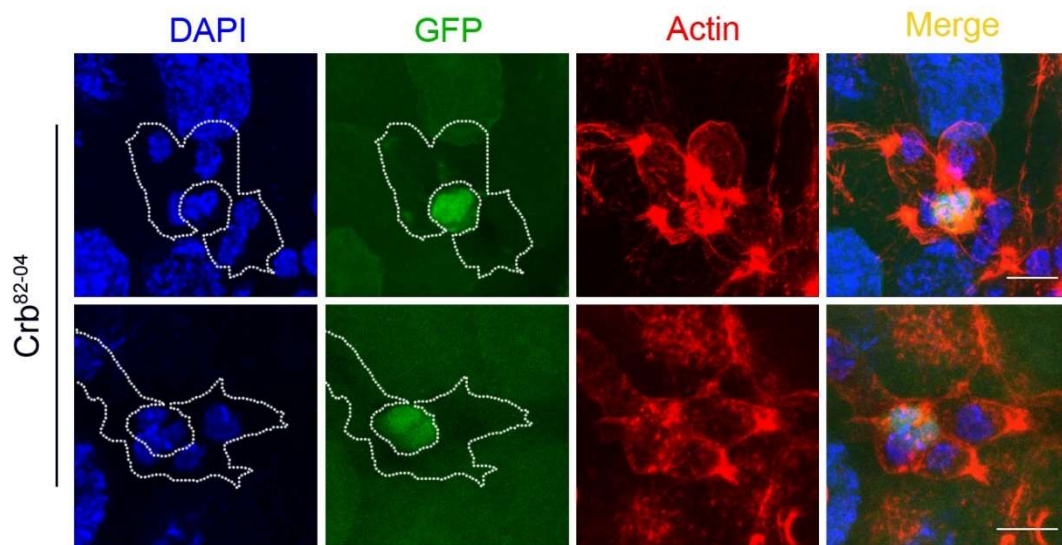


Figure S2. The *crb*⁸²⁻⁰⁴ phenotype of ectopic actin patches is autonomous to border cells. The top row and bottom row each shows a mosaic cluster containing two central polar cells that are wild type or heterozygous (GFP positive, their DAPI-labeled nuclei smaller than those of adjacent border cells). The rest of the mosaic cluster is composed of a clone of *crb*⁸²⁻⁰⁴ mutant outer border cells, which are indicated by lack of GFP and outlined by a dashed line. Wild type polar cells do not prevent the entire cluster from exhibiting the ectopic actin patches phenotype. The *crb*⁸²⁻⁰⁴ mosaic cluster shown in the top row is the same cluster shown in Fig. 1C, except that the images here are derived from maximum projection of a z-series of confocal sections but the image in Fig. 1C is

a single confocal section. The bottom mosaic cluster is also shown in Fig. 4G, and the images are all resulted from maximum projection of a z-series of confocal sections.

Scale bars: 10 μ m.

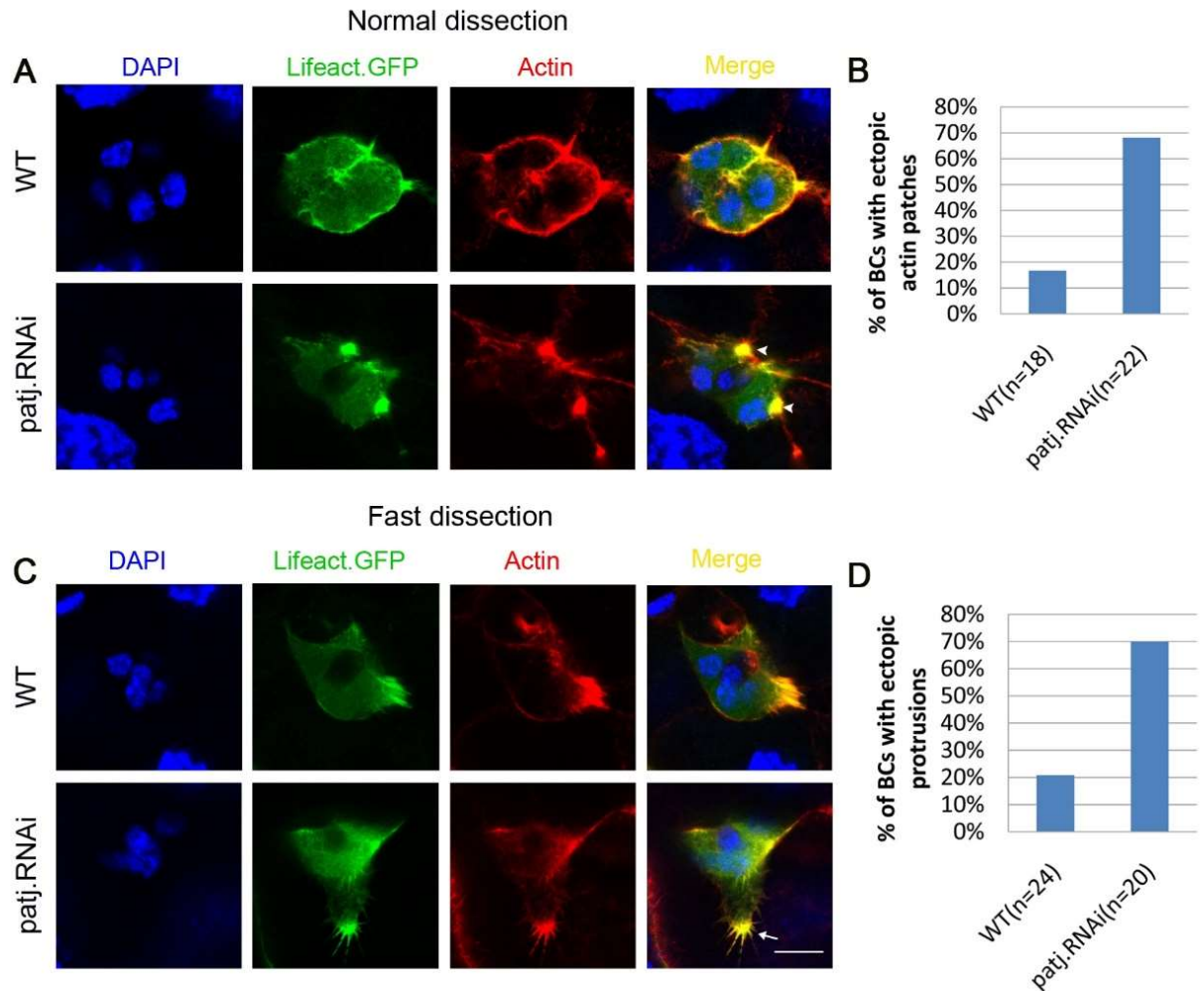


Figure S3. Fast dissection reveals fine structures of ectopic actin patches.

(A, B) After normal dissection and immunostaining (ovaries were dissected in cold PBS and the process would last about 20 minutes or above), typical wild type (WT) border cells extended a leading protrusion at the front, but *patj RNAi* border cells exhibited large ectopic actin patches at the side of cluster. Arrowheads indicate actin patches. Quantification for actin patches indicates that 68% of *patj RNAi* expressing border cell clusters (n=22) displayed ectopic actin patches. (C, D) After fast dissection and staining

(ovaries were dissected in cold PBS but the whole process was limited to less than 5 minutes), both the predominant protrusion at the leading edge in WT border cells and the ectopic actin patch in *patj* RNAi border cells exhibited finer details, which are characteristics of lamellipodial protrusion. Arrow indicates ectopic protrusion. Quantification indicates that 70% of *patj* RNAi clusters (n=20) displayed ectopic protrusions with fast method. The above results nicely confirmed that the actin patches observed using normal method are actually ectopic protrusions that displayed dynamic actin structures. F-actin is labeled by both Lifeact-GFP (green) and phalloidin-TRITC (red). Scale bar: 10 μ m.

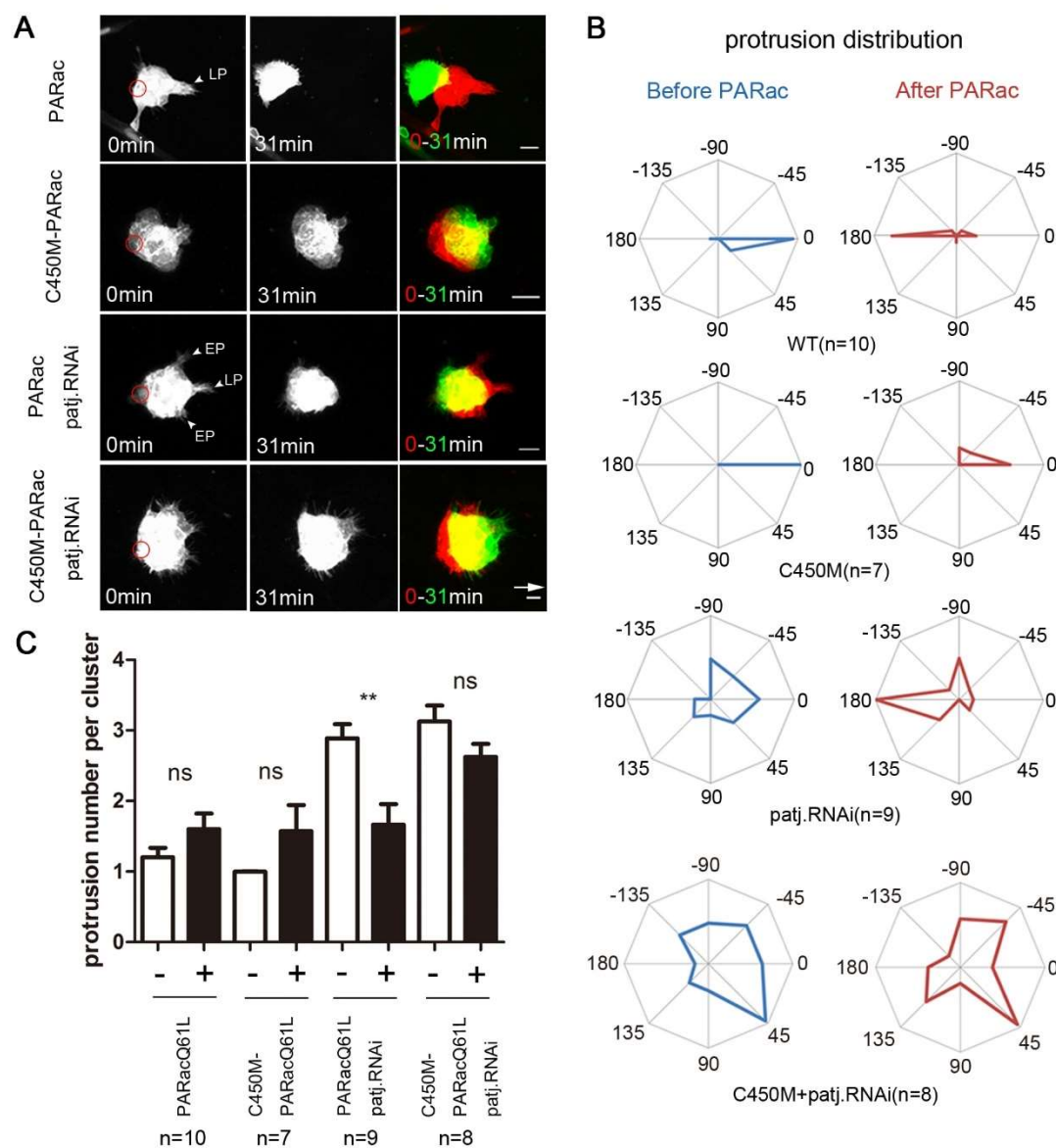


Figure S4. Loss of Patj does not affect non-autonomous cell-cell communication.

(A) Confocal images in the top panels (WT control) show that local photoactivation of PA-Rac by laser (red circle) in the back border cell induced a new protrusion, caused retraction of the leading protrusion, and redirected the whole cluster to move in an opposite direction, demonstrating effective cell-cell communication between the back cell and leading cell. The second row panels show that photoactivation of the photo-insensitive C450M-PA-Rac failed to achieve the above results, serving as a negative control (Wang et al., 2010). The third row panels show that local photoactivation of PA-Rac in the back cell of *patj RNAi* cluster not only retracted the leading protrusion but also retracted two ectopic protrusions on the side. Redirection of collective movement of cluster was also achieved. On the contrary, the bottom panels show that photoactivation of C450M-PA-Rac in *patj RNAi* background failed to result in retraction of ectopic protrusions and redirection of migration. White arrow indicates border cells' normal migration direction, which is to the right for all figures. White arrowheads point to leading protrusion (LP) and ectopic protrusion (EP). (B) Analysis of protrusion distribution by radar diagram, which divides the border cell cluster into 8 sectors. In the WT control, most of protrusions were aligned toward 0° (front) before PA-Rac photoactivation, but were switched toward 180° (back) after photoactivation. Such a switch in protrusion distribution is evident in *patj RNAi* but not in the C450M negative controls. (C) Quantification of average protrusion number per cluster reveals that a strong and significant reduction of protrusion number between before photoactivation (-) and after photoactivation (+) was only observed for *patj RNAi*. **, $P < 0.01$; ns, not significant; unpaired t-test; error bars indicate s.e.m. Scale bars: 10 μm .

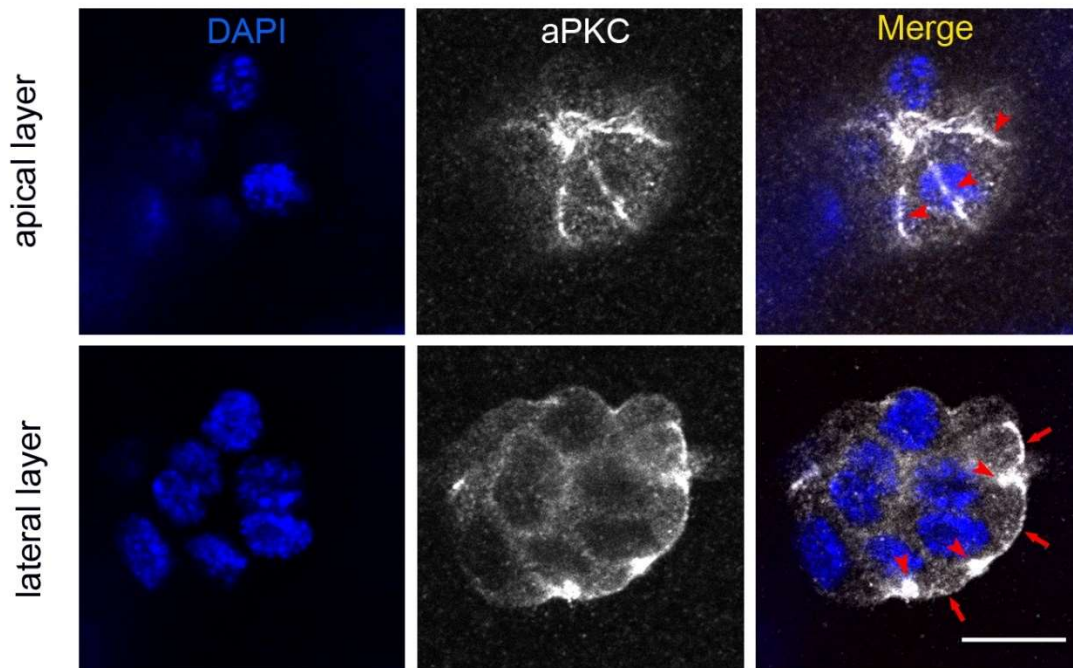


Figure S5. The two distinct pools of aPKC are best captured at two different focal planes within the same border cell cluster. The top row shows the single section confocal images of a border cell cluster at the apical layer/plane. Long lines of strong aPKC staining (indicated by red arrowheads) represent the major pool of membrane-bound aPKC at apical junctions between adjacent border cells. At this focal plane, the second minor pool of aPKC that is localized close to the outside lateral membrane is not obvious. Moving more basally to the lateral focal plane, the second pool of aPKC comes into view as thin lines or dots of moderate staining near the outside lateral membrane (indicated by red arrows) in the bottom row of confocal images. Meanwhile, the apical junctional staining of aPKC are mostly out of focus except for the remaining large spots (indicated by the red arrowheads), which are the most distal part of apical junctions between adjacent border cells. Note that between the large spots of junctional aPKC staining lies the second pool of aPKC (indicated by red arrows). Scale bars: 10 μm .

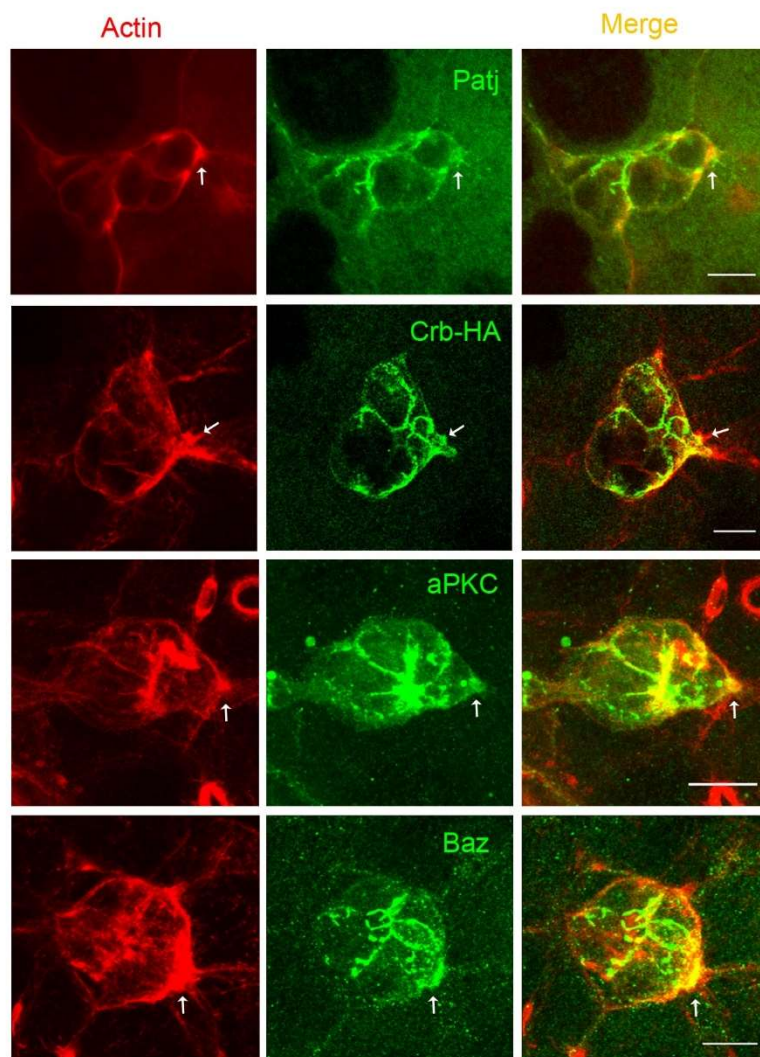


Figure S6. The second pool of apical polarity proteins is often observed to be enriched in leading protrusions. Patj, Crb-HA, aPKC and Baz are shown to be enriched (indicated by white arrows) in the leading protrusions of wild type border cell clusters. Because the apical junctional pool and the second pool near outside lateral membrane cannot be easily captured in one confocal image, we have to generate maximum projections of z-series to show both pools for Crb-HA, aPKC and Baz. The top row of Patj images is from single confocal sections, the same cluster is also shown in Fig. 3A (Patj). F-actin was labeled by phalloidin (red). Scale bars: 10 μ m.

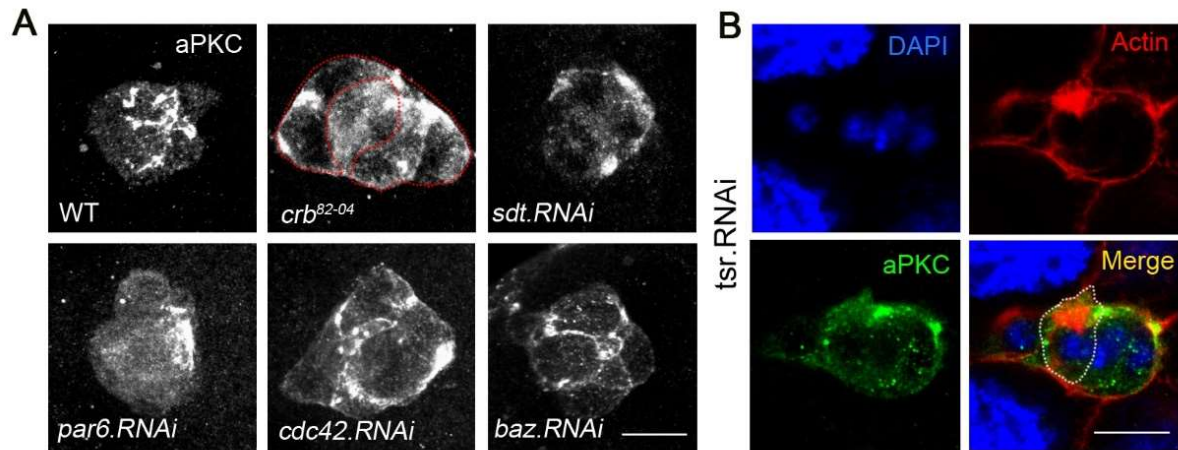


Figure S7. Distribution of aPKC caused by loss of function of Crb, Sdt, Par6, Cdc42, Baz and cofilin.

(A) Confocal images showing that loss of Crb complex components (Crb and Sdt) or Par complex components (Par6, Cdc42 but not Baz) severely disrupted the distribution of aPKC in the apical junctions. Reduction of Baz did not grossly affect the aPKC's distribution pattern. Dotted red line outlines the mutant *crb*⁸²⁻⁰⁴ clone in the cluster. (B) One border cell cluster containing a single cell flip-out clone expressing *tsr RNAi* (*tsr* encodes cofilin) resulted in a large ectopic actin patch inside the clone, but no aPKC staining was colocalized with the actin patch. Scale bars: 10µm.

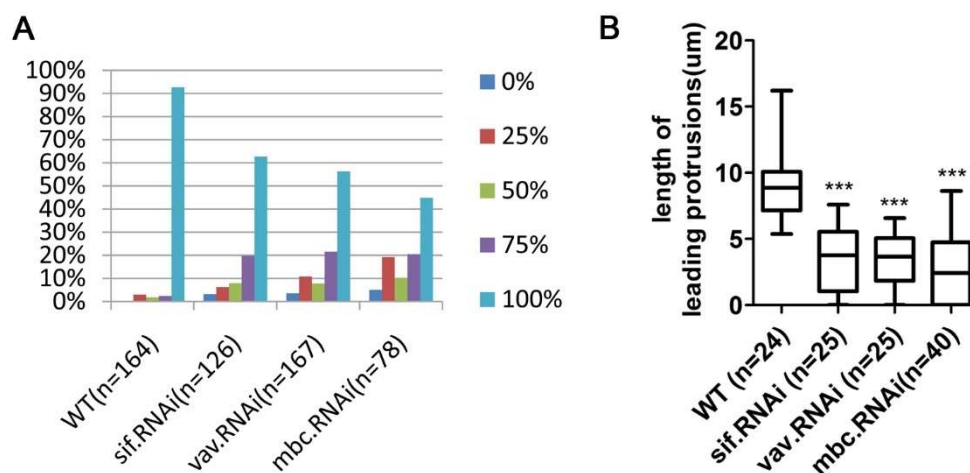


Figure S8. Knockdown of *sif*, *vav* or *mbc* resulted in migration defects and shortening of leading protrusions.

(A) *sif*, *vav*, or *mbc* RNAi each caused migration delay and (B) significant reduction of leading protrusion length, which is quantified and represented by the box and whisker plots. The box ranges from the 25th to the 75th percentiles, the whiskers represent the minimum and maximum values, and the line indicates the median value. *** $P < 0.001$; unpaired t-test.

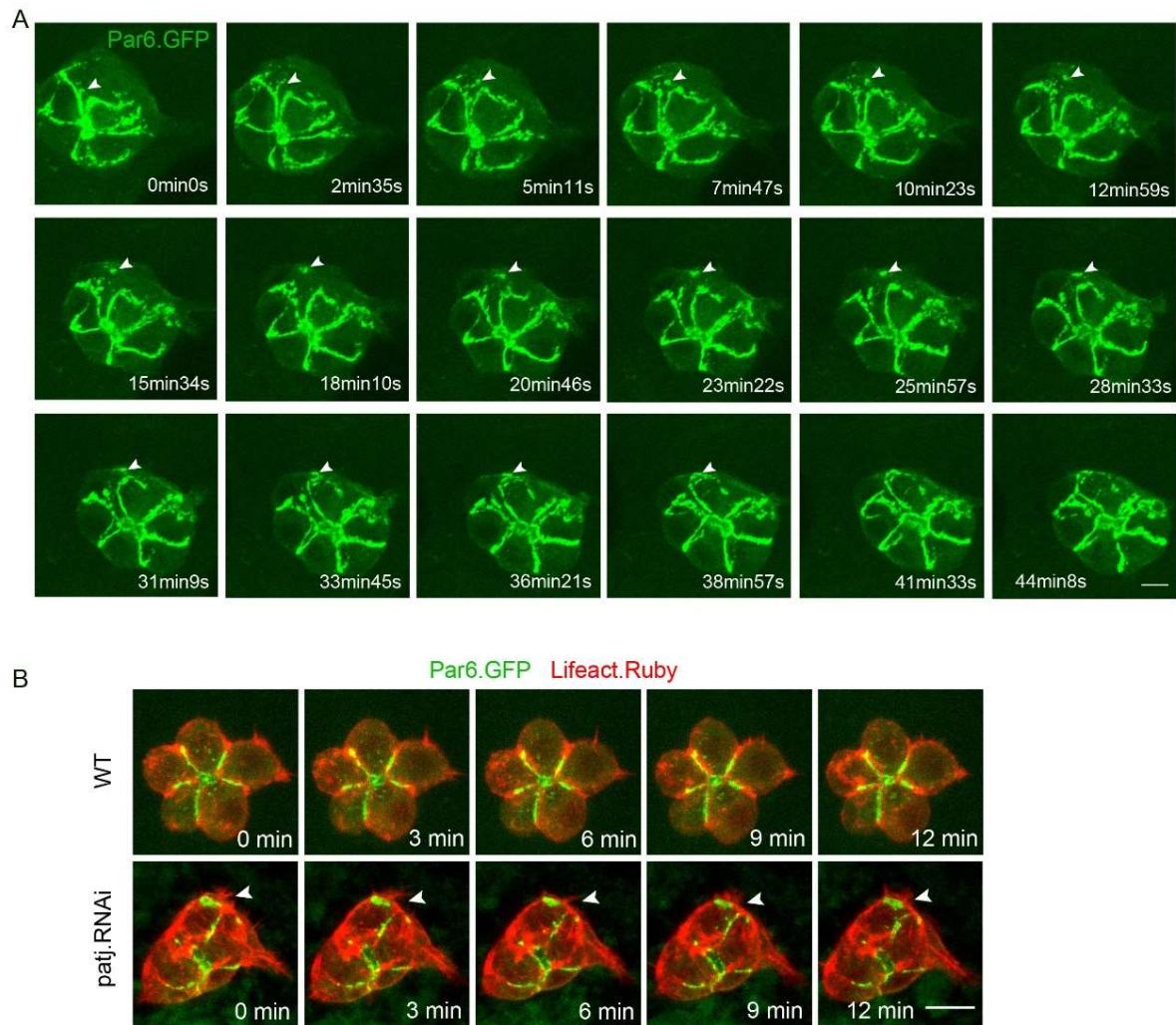


Figure S9. Dynamic distribution of Par6-GFP in WT and *patj* RNAi border cells.

(A) Time lapse images showing the dynamic distribution pattern of Par6-GFP in WT border cells. Par6-GFP signals mainly accumulated as lines at the apical junctions but they could be observed detaching from junctions as dots and moving toward the outer cortex. Arrowhead points to such a dot. (B) Time lapse images showing ectopic actin-rich protrusions extended from the position where an ectopic Par6-GFP patch was present as a result of loss of Patj (the second row), but this phenomenon could not be found in WT control (the first row). F-actin was labeled by Lifeact-Ruby (red). Arrowhead highlights the ectopic protrusion. Scale bar: 10 μ m.

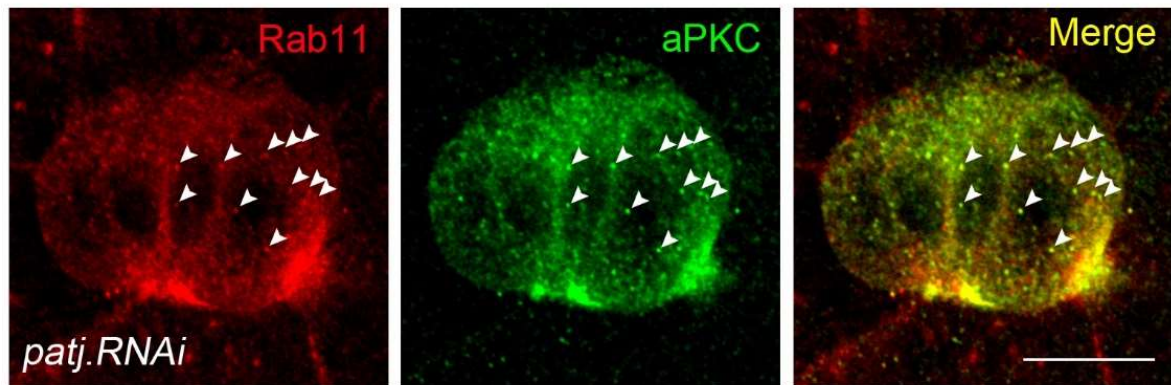


Figure S10. A high level of recycling is associated with large ectopic aPKC spots.

In *patj RNAi* border cells, locally enriched recycling vesicles/endosomes were shown to partially localize with large ectopic aPKC patches near the outside membrane. In addition, Rab11-labeled recycling vesicles were shown to clearly colocalize with small aPKC dots in the cytoplasm (colocalizations indicated by white arrowheads). The images were captured using the latest Zeiss 880 Airyscan technology for high resolution imaging (achieving a maximum resolution of 120 nm in the x-y plane according to the manufacturer, which is close to super resolution quality). Scale bar: 10 μ m.

Table S1. UAS stocks obtained from public *Drosophila* stock centers

Genotype	Stock #	Use frequency	Source
<i>UAS-patj.RNAi</i>	THU1704	++	Tsinghua University RNAi Stock Center (TURSC)
<i>UAS-patj.RNAi</i>	12021R-3	+	National Institute of Genetics (NIG)
<i>UAS-patj.RNAi</i>	31620	+	Vienna Drosophila Research Center (VDRC)
<i>UAS-patj.RNAi</i>	101877	+	VDRC
<i>UAS-sdt.RNAi</i>	THU1336	++	TURSC
<i>UAS-sdt.RNAi</i>	29844	+	VDRC
<i>UAS-sdt.RNAi</i>	15342R-2	+	NIG
<i>UAS-aPKC.RNAi</i>	THU5841	++	TURSC
<i>UAS-aPKC.RNAi</i>	105624	++	VDRC
<i>UAS-baz.RNAi</i>	5055R-1	++	NIG
<i>UAS-baz.RNAi</i>	5055R-2	++	NIG
<i>UAS-baz.RNAi</i>	2915	+	VDRC
<i>UAS-baz.RNAi</i>	2914	++	VDRC
<i>UAS-par6.RNAi</i>	19731	+	VDRC
<i>UAS-par6.RNAi</i>	THU3865	++	TURSC
<i>UAS-sif.RNAi</i>	5406R-2	++	NIG
<i>UAS-sif.RNAi</i>	5406R-3	++	NIG
<i>UAS-sif.RNAi</i>	25789	+	Bloomington Drosophila Stock Center (BDSC)
<i>UAS-vav.RNAi</i>	6241	++	VDRC
<i>UAS-mbc.RNAi</i>	TH02182.N	+	TURSC
<i>UAS-mbc.RNAi</i>	TH02150.N	++	TURSC
<i>UAS-mbc.RNAi</i>	THU0808	++	TURSC
<i>UAS-mbc.RNAi</i>	TH01095.N2	+	TURSC
<i>UAS-cdc42.RNAi</i>	12530R-2	++	NIG
<i>UAS-cdc42.RNAi</i>	12530R-3	++	NIG
<i>UAS-cdc42.RNAi</i>	29004	+	BDSC
<i>UAS-crb</i>	5544		BDSC
<i>UAS-Rab5-DN</i>	9771		BDSC
<i>UAS-Rab11-DN</i>	23261		BDSC
<i>UAS-Shi-DN</i>	108437		KYOTO Stock Center (DGRC)
<i>UAS-Shi-DN</i>	108445		DGRC
<i>UAS-clc.GFP</i>	7107		BDSC
<i>UAS-sif</i>	9127		BDSC
<i>FRT82B crb[j1B5]/TM6B</i>	111051		DGRC
<i>UAS-GFP</i>	1522		BDSC
<i>UAS-RacN17</i>	6292		BDSC
<i>UAS-patj</i>	39735		BDSC
<i>UAS-tsr.RNAi</i>	110599		VDRC
<i>UAS-Lifeact.Ruby</i>	35545		BDSC
<i>UAS-Lifeact.GFP</i>	35544		BDSC

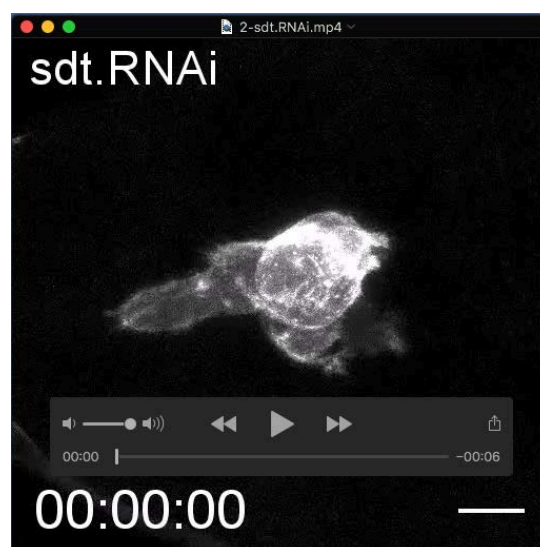
++ RNAi stocks more frequently used in this study.

+ RNAi stocks sometimes used in this study.

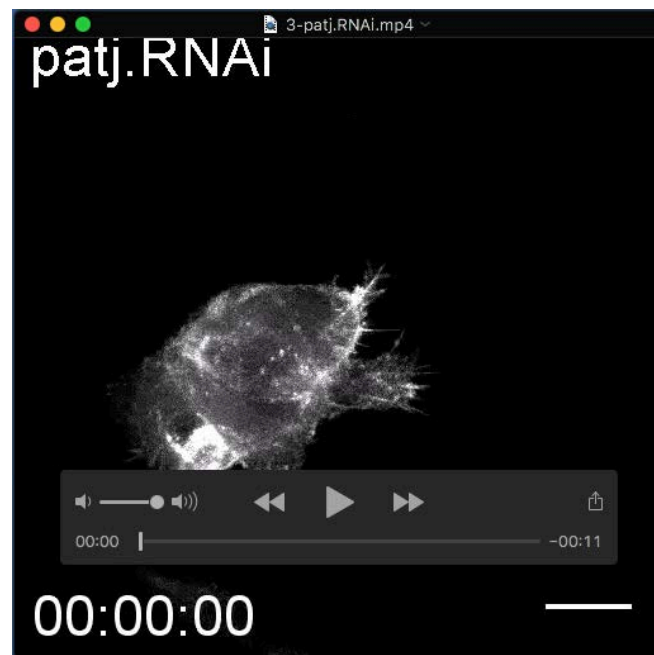
Movies



Movie 1. Live imaging of collective migration of a wild type (WT) border cell cluster. The border cells are shown migrating as a coherent cluster, with a large, predominant protrusion at the leading position. UAS-lifeact-GFP was expressed to label F-actin enriched structures such as protrusions in this and all subsequent movies. See Materials and Methods for details on live imaging. Scale bar: 10 μ m.



Movie 2. Live imaging of migrating border cells that are expressing *sdt RNAi*. The border cell cluster is shown extending several large ectopic protrusions during migration. The genotype of border cells is *slbo-Gal4, UAS-sdt RNAi, UAS-Lifeact-GFP*. All the transgenes and *RNAi* constructs were expressed using *slbo-Gal4*, a border cell-specific *Gal4* driver in this and subsequent movies. Scale bar: 10 μ m.



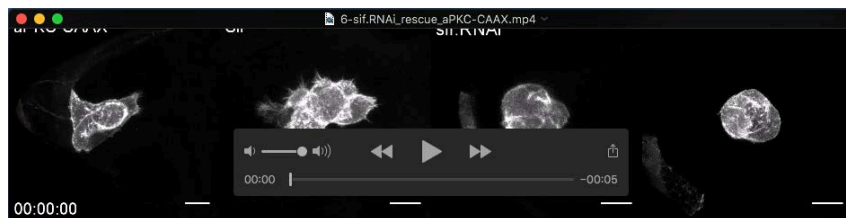
Movie 3. Live imaging of collective migration of *patj RNAi* expressing border cells. The *patj RNAi* border cells extend several ectopic protrusions in random directions during migration. Scale bar: 10 μ m.



Movie 4. Additional expression of *aPKC-DN* or *sif RNAi* rescues the ectopic protrusions phenotype exhibited by *patj RNAi* expression. Reducing the function of aPKC (by *aPKC-DN* expression), or Sif (by *sif RNAi* expression), in the background of *patj RNAi* expression, rescued the phenotype of ectopic protrusions. Note that the leading protrusions are also significantly shortened. Scale bars: 10 μ m.



Movie 5. Live imaging of border cell clusters expressing different mutant forms of aPKC. Expressing the dominant negative form of aPKC (aPKC-DN) resulted in suppression of leading protrusion formation, even though dynamic filopodial structures were seen forming randomly. In contrast, expression of the overactivated forms of aPKC (aPKC-CAAX and aPKC-CA) resulted in formation of large ectopic protrusions. Their clusters are much less coherent than the wild type clusters, individual border cells appear stretched outward. Scale bars: 10 μ m.



Movie 6. Sif overexpression resembles the aPKC-CAAX phenotype while *sif RNAi* rescues aPKC-CAAX's phenotype. Sif overexpression resembles the aPKC-CAAX phenotype that displays large ectopic protrusions and outstretched border cells. Expression of *sif RNAi* rescues aPKC-CAAX's phenotype. Scale bars: 10 μ m.



Movie 7. Expression of aPKC-DN fails to rescue the ectopic protrusions phenotype of Sif overexpression. Co-expression of the dominant negative form of aPKC (aPKC-DN) with Sif resulted in the same phenotype of expressing Sif alone. Scale bars: 10 μ m.